We are IntechOpen, the world's leading publisher of Open Access books Built by scientists, for scientists

6,900
Open access books available

186,000
International authors and editors

200M
Downloads

Our authors are among the

154
Countries delivered to

TOP 1%
most cited scientists

12.2%
Contributors from top 500 universities

WEB OF SCIENCE™

Selection of our books indexed in the Book Citation Index in Web of Science™ Core Collection (BKCI)

Interested in publishing with us?
Contact book.department@intechopen.com

Numbers displayed above are based on latest data collected.
For more information visit www.intechopen.com

16

Pulse-Shaping Techniques Theory and Experimental Implementations for Femtosecond Pulses

T. Oksenhendler and N. Forget
Fastlite, Centre scientifique d'Orsay – Bât 503
Plateau du Moulon – BP45, 91401 ORSAY
France

1. Introduction

Femtosecond pulses are used in many fields due to their specificities of extreme short duration, ultra high peak power or large spectral bandwidth.
Since the early days of the laser in the 60s, there has been a continous quest to generate shorter and or higher peak power pulses.
Reliable generation of pulses below 100fs occurred the first time in 1981 with the invention of the colliding pulse modelocked (CPM) ring dye laser (Fork R.L. and al., 1981). Despite relative low energy per pulses, the ultrashort pulse duration leads to peak power large enough for non linear pulse compression culminating in pulses as short as 6fs in the visible. Recent advances in laser technology as the use of solid-state gain media, laser diode pumping, fiber laser, have led to simple, reliable, turn key ultrashort laser oscillators with pulse duration ranging form few ps down to 5fs.
Limitation to pulse energy in the range of a microJoule or less in the CPM laser has been overcomed by the Chirped Pulse Amplification (CPA) technique (Strickland D., Mourou G., (1985)). This technique is the optical transposition of a Radar technique developped during the second world war. The basic principle is to spread in time i.e to stretch the ultrashort pulse before amplification. Indeed limitation of the pulse amplification because of the damage threshold of the optics is mainly due to the pulse peak power. A stretch ratio of a million gives the ability to amplify the stretched pulse, without optical damage, by a factor of a million from less than a microJoule to more than a Joule per pulse. After amplification, recompression of the pulse is achieved by an optical set-up that has a very high damage threshold. To obtain the highest peak power, the pulse duration has to be "Fourier transform limited", ie its spectral phase is purely linear. The compensation of the chirp and higher spectral phase order is highly simplified by the ability to introduced an arbitrarly shaped spectral phase.
Application of these ultrashort pulses requires to control of optimize their temporal shape. Dispersion of materials and optical devices has been used to compress, stretch or replicate the pulses. Limitations on the ability to control the pulse temporal shape by classical optical devices have lead to the development of arbitrary pulse shapers. These devices are linear

Source: Advances in Solid-State Lasers: Development and Applications, Book edited by: Mikhail Grishin,
ISBN 978-953-7619-80-0, pp. 630, February 2010, INTECH, Croatia, downloaded from SCIYO.COM

filters enabling the independent control of the spectral amplitude and phase giving a complete control of the temporal shape of the pulse.
Due to the extreme short duration of the pulses, the temporal control cannot be achieved directly by temporal modulators. The control has to be done in the spectral domain. Two technologies of pulse shapers are widely used: spatial amplitude and phase modulators implemented in a zero-dispersion line or 4-f line, and acousto-optic programmable dispersive filters based on longitudinal Bragg acousto-optic diffraction.
Both techniques will be theoretically reviewed to point out limitations, advantages and drawbacks for femtosecond pulse shaping techniques. Starting from simulations of the two techniques, some specific examples of pulse shaping will be invastigated such as pulse compression, complex square pulse generation, pure linear chirp generation, double pulses with a controlled delay or focal point power density optimization. These examples will then be used to illustrate the limitations, advantages and drawbacks of each technology.
Experimental implementations of these pulse shaping examples will then be briefly presented.
In the last section, we discuss some special topics, Carrier Enveloppe Phase control and indirect pulse shaping.

2. Ultrashort pulses characteristics

The extreme shortness of ultrashort pulses implies a large spectral bandwidth. The temporal and spectral electric fields are dual i.e. Fourier transform. Thus the electric field can be determined either by the temporal phase and amplitude or by the spectral phase and amplitude.
The electric field is a real quantity that can be decomposed as:

$$\mathcal{E}(\mathrm{t})=\frac{1}{2}\left[\mathrm{E}(\mathrm{t})+\mathrm{E}^{*}(\mathrm{t})\right] \tag{1}$$

with E(t) the complex electric field whose corresponds to positive frequency. This field can be expressed as:

$$E(t) = A(t)\, e^{-i\omega_0 t + i\varphi(t)} \tag{2}$$

where ω_0 is the central pulsation, A(t) its enveloppe and φ(t) its temporal phase.
Its Fourier transform corresponds to the spectral components:

$$E(\omega) = A(\omega)\, e^{i\phi(\omega)} = TF\left[E(t)\right]_{\omega} \tag{3}$$

where A(ω) is the spectral amplitude, and ϕ(ω) the spectral phase.
The spectrum I(ω), or spectral power density, is the square modulus of the spectral amplitude. Its temporal equivalent, the temporal intensity I(t) equals the square modulus of the temporal amplitude A(t).
One must be aware that the temporal amplitude A(t) depends upon both the spectral amplitude and phase.
We assume a normalized field:

$$\int_{-\infty}^{+\infty} |E(\omega)|^2 \frac{d\omega}{2\pi} = \int_{-\infty}^{+\infty} |E(t)|^2 \, dt = 1 \tag{4}$$

The pulse center is then defined by:

$$t_0 = \langle t \rangle = \int_{-\infty}^{+\infty} t \, |E(t)|^2 \, dt \tag{5}$$

The pulse duration by:

$$\Delta t = \sqrt{\langle t^2 \rangle - \langle t \rangle^2} = \sqrt{\langle (t - t_0)^2 \rangle} \tag{6}$$

The central frequency by:

$$\omega_0 = \langle \omega \rangle = \int_{-\infty}^{+\infty} \omega \, |E(\omega)|^2 \, \frac{d\omega}{2\pi} \tag{7}$$

The spectral width or bandwidth by:

$$\Delta\omega = \sqrt{\langle \omega^2 \rangle - \langle \omega \rangle^2} = \sqrt{\langle (\omega - \omega_0)^2 \rangle} \tag{8}$$

Duration and bandwidth are related by:

$$\Delta\omega \Delta t \geq \frac{1}{2} \tag{9}$$

The minimum is obtained for a pure linear spectral phase. As shown by the relations between spectral phase and duration:

$$\langle t \rangle = \int_{-\infty}^{+\infty} t |E(t)|^2 \, dt = \left\langle \frac{d\phi}{d\omega} \right\rangle, \tag{10}$$

$$\tau_g = \frac{d\phi}{d\omega}, \tag{11}$$

$$\langle t \rangle^2 = \Delta t_{\varphi=0}{}^2 + \Delta \tau_g{}^2 \text{ with } \Delta \tau_g{}^2 = \left\langle \left(\tau_g - \langle \tau_g \rangle \right)^2 \right\rangle = \left\langle \left(\frac{d\phi}{d\omega} - \left\langle \frac{d\phi}{d\omega} \right\rangle \right)^2 \right\rangle. \tag{12}$$

For $|E(\omega)|$ fixed, the pulse is shortest when τ_g is independent of the frequency ($\Delta\tau_g$=0). The pulse is said to be a Fourier transform pulse or Fourier transform limited.
By opposition when τ_g changes linearly with frequency, the pulse is said to be chirped (as when a bird sings).
To analyse the different effects of the spectral phase, it is used to expand the spectral phase into a Taylor series:

$$\phi(\omega) = \phi(\omega_0) + \phi^{(1)}(\omega_0)(\omega - \omega_0) + \frac{\phi^{(2)}(\omega_0)}{2!}(\omega - \omega_0)^2 + \frac{\phi^{(3)}(\omega_0)}{3!}(\omega - \omega_0)^3 \text{ with } \phi^{(k)}(\omega_0) = \left. \frac{\partial^k \phi(\omega)}{\partial \omega^k} \right|_{\omega_0} \tag{13}$$

The first order spectral phase term corresponds to a delay, the second order (also named chirp) spreads linearly in time the frequency and so stretches the pulse. The third order introduces pre-pulses or post-pulses around the main pulse.
Different set-ups combining gratings, prisms or grisms and optics can modify the spectral phase but not arbitrarily. The different orders cannot be set independently.
The temporal intensity is modified by changing the spectral phase only, but its complete control requires shaping both the spectral phase and amplitude. This kind of control is expressed by a linear filtering.

3. Linear filtering

The femtosecond pulse shaping approach described in this article is based on the linear, time-invariant filter, a concept well-known in electrical engineering. Here we apply linear filtering to generate specially shaped optical waveforms on the picosecond and femtosecond time scale.
Linear filtering can be described in either the time domain or frequency domain, as depicted in figure 1. In the time domain, the filter is characterized by an impulse response function h(t). The output of the filter $E_{out}(t)$ in response to an input pulse $E_{in}(t)$ is given by the convolution of $E_{in}(t)$ and h(t)

$$E_{out}(t) = E_{in}(t) \otimes h(t) = \int E_{in}(t')h(t-t')dt' \tag{14}$$

where $\otimes$ denotes convolution. If the input is a delta function, the output is simply h(t). Therefore, for a sufficiently short input pulse, the problem of generating a specific output pulse shape is equivalent to the task of fabricating a linear filter with the desired impulse response. Note that instead of the term "impulse response function", which is common in electrical engineering, h(t) may also be called a Green function, which is a common terminology in other fields.

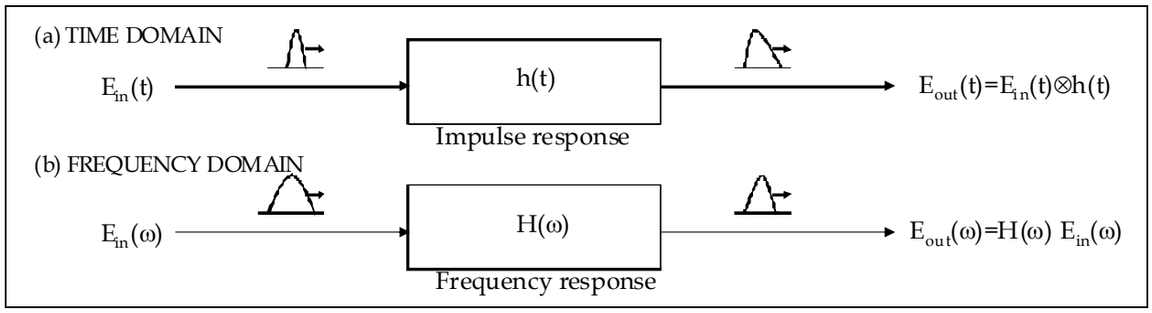

Fig. 1. Pulse shaping by linear filtering. (a) Time domain view. (b) Frequency domain view

In the frequency domain, the filter is characterized by its frequency response H(ω). The output of the linear filter $E_{out}(\omega)$ is the product of the input signal $E_{in}(\omega)$ and the frequency response H(ω) –i.e.,

$$E_{out}(\omega) = E_{in}(\omega)H(\omega) \tag{15}$$

Here $E_{in}(t)$, $E_{out}(t)$, h(t), and $E_{in}(\omega)$, $E_{out}(\omega)$, H(ω), respesctively, are Fourier transform pairs.

A linear filter can emulate any linear combination of pulses such as for examples two, three, four… pulses. Any optical system without frequency conversion or time-dependant component is indeed a linear filter (Michelson or Mach-Zender interferometers, bandpass filters, …).
For a delta function input pulse $E_{in}(t)$, the input spectrum $E_{in}(\omega)$ is equal to unity, and the output spectrum is equal to the frequency response of the filter. Therefore, due to the Fourier transform relations, generation of a desired ouput waveform can be accomplished by implementing a filter with the required frequency response. As the time scale of the pulses (10fs-100fs) is shorter than any temporal modulator (>10ps), the pulse shaping approach is based on frequency domain and naturally is described by frequency domain point of view.

4. Theory of Pulse shaping techniques

The two main technologies of pulse shaping commonly used are the 4-f pulse shaper, or Fourier transform femtosecond pulse shaping, and the acousto-optic programmable dispersive filter (AOPDF). This part will review theoretically these two technologies and introduces their simulation models in order to determine the frequency response of these filters.

4.1 Femtosecond pulse shaping using spatial light modulators

4.1.1 Analytical analysis

The first use of the pulse shaping apparatus shown in Fig.2 was reported by Froehly, who performed pulse shaping experiments with 30ps input pulses [Froehly (1983)]. Related experiments demonstrating shaping of a few picoseconds pulses by spatial masking within a fiber and grating compressor were performed independently by Heritage and Weiner in 1985. In those experiments a grating pair was used in a dispersive configuration without internal lenses since grating dispersion was needed in order to compress the input pulses which were chirped through non linear propagation in the fiber. The dispersion-free apparatus in Fig.2 was subsequently adopted by Weiner et al. for manipulating pulses on the 100fs time scale, initially using fixed masks and later using programmable Spatial Light Modulators (SLM). The apparatus of Fig. 2 (without the mask) can also be used to introduce dispersion for pulse stretching or compression by changing the grating-lens spacing. This idea was introduced and analyzed by Martinez and is now extensively used for high-power femtosecond chirped pulse amplifier.
The waveform synthesis is achieved by spatial masking of the spatially dispersed optical frequency spectrum. Figure 2 shows the basic pulse shaping apparatus, which consists of a pair of diffraction gratings and lenses, arranged in a configuration known as a "zero dispersion pulse compressor", and a pulse shaping mask. The individual frequency components contained within the incident ultrashort pulse are angularly dispersed by the first diffraction grating, and then focused to small diffraction limited spots at the back focal plane of the first lens, where the frequency components are spatially separated along one dimension. Essentially the first lens performs a Fourier transform which converts the angular dispersion from the the grating to a spatial separation at the back focal plane. Spatially patterned amplitude and phase masks (or a SLM) are placed in this plane in order to manipulate the spatially dispersed optical Fourier components. After a second lens and grating recombine all the frequencies into a single collimated beam, a shaped output pulse is

obtained, with the output pulse shape given by the Fourier transform of the patterned transferred by the masks onto the spectrum.

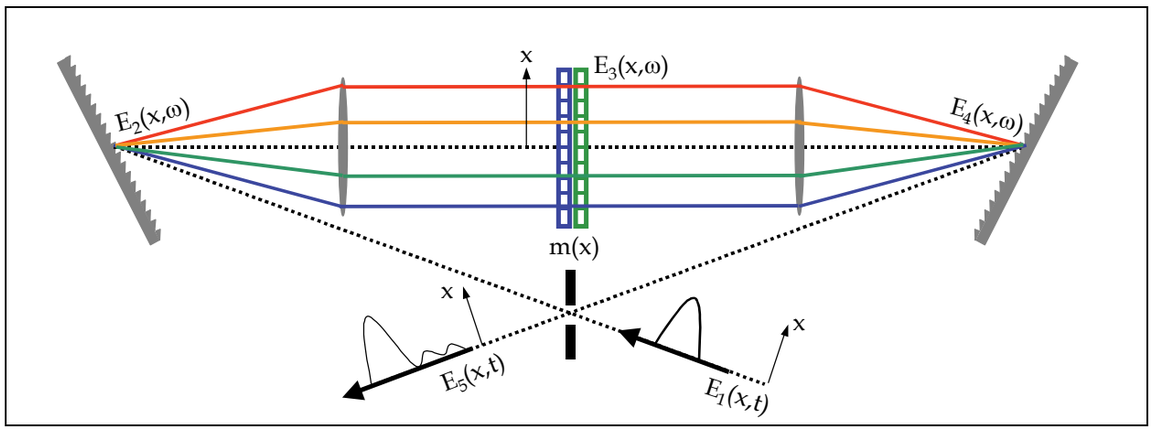

Fig. 2. Basic layout for Fourier transform femtosecond pulse shaping.

In order for this technique to work as desired, one requires that in the absence of a pulse shaping mask, the output pulse should be identical to the input pulse. Therefore, the grating and lens configuration must be truly free of dispersion. This can be guaranteed if the lenses are set up as a unit magnification telescope. In this case the first lens performs a spatial Fourier transform between the plane of the first grating and the masking plane, and the second lens performs a second Fourier transform from the masking plane to the plane of the second grating. The total effect of these two consecutive Fourier transforms is that the input pulse is unchanged in traveling through the system if no pulse shaping mask is present.
Note that this dispersion-free condition also depends on several approximations, e.g., that the lenses are thin and free of aberrations, that chromatic dispersion in passing through the lenses or other elements which may be inserted into the pulse shaper is small, and that the gratings have a flat spectral response. Many optimized designs have been proposed in the litterature to minimize optical aberrations [Monmayrant and Chatel (2003), Weiner(2000),…].
The optimization of the apparatus for a quantitative control requires precise analysis and simulation[Wefers and Nelson (1995), Vaughan and al (2006), Monmayrant (2005)]. In terms of the linear filter formalism, we wish to relate the linear filtering function H(ω) to the actual physical masking function with complex transmittance m(x). To do so, we must determine the relation between the spatial dimension x on the mask and the optical frequency ω. The input grating disperses the optical frequencies angularly:

$$\lambda = p\left(\sin\theta_i + \sin\theta_d\right) \tag{16}$$

where λ is the optical wavelength, p is the spacing between grating lines, and θ_i and θ_d are angles of incidence and diffraction, respectively. The first lens brings the diffracted rays from the first grating parallel. The lateral displacement x of a given frequency component λ from the center frequency component λ_0 immediately after the lens is given by

$$x(\lambda) = f\tan\left[\theta_d(\lambda) - \theta_d(\lambda_0)\right] \tag{17}$$

Expanding x as a power series in angular frequency ω gives

$$x(\omega) = f\left[\left.\frac{\partial\theta_d}{\partial\omega}\right|_{\omega=\omega_0}(\omega-\omega_0) + \frac{1}{2}\left.\frac{\partial^2\theta_d}{\partial\omega^2}\right|_{\omega=\omega_0}(\omega-\omega_0)^2 + \ldots\right], \tag{18}$$

where

$$\left.\frac{\partial\theta_d}{\partial\omega}\right|_{\omega=\omega_0} = \frac{2\pi c}{\omega_0{}^2 p\cos\theta_d(\omega_0)} \text{ and } \left.\frac{\partial^2\theta_d}{\partial\omega^2}\right|_{\omega=\omega_0} = \frac{-4\pi c}{\omega_0{}^3 p\cos\theta_d(\omega_0)}, \tag{19}$$

c is the speed of light, and ω_0 is the central carrier frequency of the input pulse.
Usually the second order term is neglected [except in Monmayrant thesis and Vaughan and al.] so that the frequency components are laterally dispersed linearly across the mask. However, for very broad bandwidth pulses (pulse with duration <20fs), or precise pulse shaping, this assumption may break down. Subtle second order dispersion effects have been noticed by Weiner and co-workers[Weiner (1988)], and Sauerbrey and co- workers[Vaughan (2006)].
It is assumed that the lateral dispersion of the lenses and gratings is such that the mask can accommodate the entire bandwidth of the input pulse. The "mask bandwidth" depends upon the width of the mask L, the focal length of the lens f, the line spacing of the grating p and the angle of diffraction $\theta_d(\omega_0)$:

$$\Delta\lambda_M = \arctan\left(\frac{L}{f}\right) p\cos\theta_d(\omega_0). \tag{21}$$

To avoid any significant cut, the "mask bandwidth" $\Delta\Omega_M$ has to be larger than the input pulse bandwidth $\Delta\omega$. We shall use as a criteria that $\Delta\Omega_M > 3\Delta\omega$.
Considering an ideal mask, without pixelisation and other spurious effect, the space-time coupling used for the temporal or spectral shaping by a spatial mask has some incidence on the shaped pulse [Danailov (1989), Wefers (1995), Wefers (1996), Sussman (2008)]. The principal issue is that the spectral content – and hence time evolution – at each point within the output beam is not the same. Following the notations introduced on Fig.2 and by considering the input field without space-time coupling, the electric field incident upon the pulse shaping apparatus (immediately prior to the grating) is defined in the slowly varying envelope approximation as

$$E_1(x,t) = E_{in}(x)A(t)e^{-i\omega_0 t + i\varphi(t)}. \tag{22}$$

Following the results of Martinez [Martinez (1986)], the electric field immediately after the grating in frequency and position space is given by

$$E_2(x,\Omega) = \sqrt{\beta}E_{in}(\beta x)A(\Omega)e^{i\gamma\Omega x + i\phi(\Omega)} \tag{23}$$

with $\beta = \cos\theta_i / \cos\theta_d$, $\gamma = 2\pi / \omega_0 p\cos\theta_d$, and $\Omega = \omega - \omega_0$, where $\phi(\Omega) = \phi(\omega)$ and θ_i and θ_d are the angles of incidence and diffraction respectively, and p the grating line spacing.
The electric field profile in the focal plane of the lens is given by the spatial Fourier transform of (23) with the substitution $k = 2\pi x/\lambda_0 f$, where f is the focal length of the lens and λ_0 is the center wavelength of the input field. The electric field is then multiplied by the mask filter m(x) to give

$$E_3(x,\Omega) = \sqrt{2\pi / \beta\lambda_0 f}\,\tilde{E}_{in}\left(2\pi x / \beta\lambda_0 f + \gamma\Omega / \beta\right) A(\Omega) e^{i\phi(\Omega)} m(x) \tag{24}$$

where $\tilde{E}_{in}(k)$ is the spatial fourier transform of $E_{in}(x)$.
To determine the electric field profile immediately before the second grating, a spatial Fourier transform of Eq.(24) is taken again with the substitution $k=2\pi x/\lambda_0 f$, giving

$$E_4(x,\Omega) = \left(\sqrt{2\pi\beta} / \lambda_0 f\right)\left[E_{in}(-\beta x) A(\Omega) e^{i\phi(\Omega) - i\gamma\Omega x} \otimes M(2\pi x / \lambda_0 f)\right] \tag{25}$$

where $M(k)$ is the spatial Fourier transform of the mask pattern m(x) and $\otimes$ denotes a convolution.
Again following Martinez, the inverse transfer function of the second grating (which is anti-parallel to the first) gives the electric field profile after the grating as

$$E_5(x,\Omega) = \left(\sqrt{2\pi} / \beta\lambda_0 f\right)\left[E_{in}(-x) A(\Omega) e^{i\phi(\Omega) - i\gamma\Omega x/\beta} \otimes M(2\pi x / \beta\lambda_0 f)\right] \tag{26}$$

Taking the spatial Fourier transforms of (26) yields the electric field profile of the output waveform in the spatial frequency domain

$$\tilde{E}_{out}(k,\Omega) = \tilde{E}_5(k,\Omega) = \tilde{E}_{in}(-k,\Omega) m\left(\lambda_0 f\left(\gamma\Omega + \beta k\right)\right) = \tilde{E}_{in}(-k) A(\Omega) e^{i\phi(\Omega)} m\left(\lambda_0 f\left(\gamma\Omega + \beta k\right)\right). \tag{27}$$

In space and time it is expressed as a convolution

$$E_{out}(x,t) = \left(\sqrt{2\pi}/\gamma\lambda f\right) e^{i\omega_0 t} \int E_{in}\left(-\left(x + t\beta/\gamma\right), t - t'\right) M\left(-2\pi t'/\gamma\lambda f\right) dt'. \tag{28}$$

The space-time coupling appears as a coupling between the spatial and spectral frequencies onto the mask. If the mask does not modify the beam, it cancels out. But if the mask introduces a modulation then the output pulse will be modified both on its spectral and spatial dimensions. Due to this coupling, no simple expression of the pulse shaper response function H(ω) can be given without the strong hypothesis that this effect is negligeable.
To illustrate this effect, we will consider a pure delay, and a quadratic phase sweep to compensate for an initial chirp of the input pulse.
For a pure delay, the spectral phase is linear and the mask is given by

$$m(\omega) = e^{-i\omega\tau}. \tag{29}$$

Applying eq. (27) with this mask and an inverse spatial Fourier transform yields the output electric field

$$E_{out}(x,\Omega) = E_5(x,\Omega) = E_{in}\left(x + \left(\beta/\gamma\right)\tau\right) A(\Omega) e^{i\phi(\Omega) - i\omega\tau}. \tag{30}$$

The output beam is spatially shifted and this shift is proportionnal to the applied delay. Quantitavely, the slope of this time-dependent lateral shift is given by

$$v = \partial x/\partial t = -\beta/\gamma = {-cp\cos\theta_i}\big/{\lambda}, \tag{31}$$

Which for typical parameters (p=1000-line/mm gratings, λ=800nm) is ≈0.2mm/ps. Equation (31) shows that this slope depends only on the angular dispersion produced by the grating.

However, the effect of this lateral shift is measured relative to the spot size of the unshaped incident pulse. Spatially large input pulses reduce the effect of space time coupling but also reduce the spot size on the mask.
We now consider a mask pattern consisting of a quadratic phase sweep

$$m(\omega) = e^{-\frac{i}{2}\phi^{(2)}\Omega^2}. \tag{32}$$

This quadratic spectral phase sweep produces a "chirped" pulse with a temporally broadened envelope and an instantaneous carrier frequency that varies linearly with time under that envelope. The delay associated with each spectral components varies linearly ($\tau(\Omega)=\phi^{(2)}\Omega$). So from Eq.(30), by replacing τ by $\tau(\Omega)$, the spatial dependance becomes coupled with the optical frequency. Exact calculations have been done by Wefers[1996] and Monmayrant [2005]. These analyses point out a complex spatio-temporal coupling modifying the beam divergence and even the compression of the initial pulse. Supposing that the initial pulse has gaussian shapes in space and spectral amplitude, and is "chirped" as

$$E_{in}(x,\Omega) = E_{in}(x)A(\Omega)e^{i\frac{\phi_{in}^{(2)}}{2}\Omega^2} = e^{-x^2/\Delta x^2}e^{-\Omega^2/\Delta\Omega^2}e^{-i\frac{\phi_{in}^{(2)}}{2}\Omega^2}. \tag{33}$$

$$E_{in}(x,t) \propto e^{-x^2/\Delta x^2}\exp\left(-\left(\left(1/\Delta\Omega^2\right)-i\left(\phi_{in}^{(2)}/2\right)\right)\Big/4\left(\left(1/\Delta\Omega^2\right)^2+\left(\phi_{in}^{(2)}/2\right)^2\right)t^2\right). \tag{34}$$

Then the effect of the pulse shaper should be to recompress this pulse to its best compressed pulse

$$E_{out,best\ compressed}(x,t) \propto e^{-x^2/\Delta x^2}e^{-\Delta\Omega^2 t^2/4}. \tag{35}$$

The exact calculation with the spatio-temporal coupling yields to

$$E_{out}(x,t) \propto e^{-\Phi_x x^2}e^{-\Phi_t t^2}e^{\Phi_{xt}xt}e^{iX_x x^2}e^{iX_t t^2}e^{-iX_{xt}xt}, \tag{36}$$

where $\Phi_x = \left(1/\Delta x_p{}^2\right)$, $\Phi_t = \left(\left(1/\Delta\Omega^2\right)+\left(v^2\phi^{(2)2}/\Delta x_p{}^2\right)\right)\Big/4\Delta$,

$\Phi_{xt} = \left(\left(A\phi^{(2)}/v\right)\left(\left(1/\Delta\Omega^2\right)+\left(v^2\phi^{(2)2}/\Delta x_p{}^2\right)\right)+\left(v\phi^{(2)}/\Delta x_p{}^2\right)\left(\phi^{(2)}+\phi_{in}^{(2)}+2A\phi^{(2)2}/2\right)\right)\Big/4\Delta$, $X_x = A/v^2$,

$X_{xt} = \left(\left(v\phi^{(2)}/\Delta x_p{}^2\right)\left(\left(1/\Delta\Omega^2\right)+\left(v^2\phi^{(2)2}/\Delta x_p{}^2\right)\right)-\left(\left(\alpha\phi^{(2)}/v\right)\right)\left(\phi^{(2)}+\phi_{in}^{(2)}+2\alpha\phi^{(2)2}/2\right)\right)\Big/4\Delta$, and

$\Delta = \left(\left(1/\Delta\Omega^2\right)+\left(v^2\phi^{(2)2}/\Delta x_p{}^2\right)\right)^2+\left(\phi^{(2)}+\phi_{in}^{(2)}+2A\phi^{(2)2}/2\right)^2$, $v=-\beta/\gamma=-pc\cos\theta_i/\lambda_0$,

$A = \left(2\phi^{(2)}\right)\Big/\left(\left(2\phi^{(2)}\right)^2+\left(\Delta x^2/v^2\right)^2\right)$, $\Delta x_p = \Delta x\sqrt{\left(1+\left(2v^2\phi^{(2)}/\Delta x^2\right)\right)}$, $\theta = -\arctan\left(2\phi^{(2)}v^2/\Delta x^2\right)$.

This equation illustrates the degree of complexity of the spatio-temporal coupling. The pulse temporal ans spatial characteristics are modified by the pulse shaping. The temporal amplitude and phase are altered through respectively Φ_t and X_t. The spatial properties are affected through the dependance of Φ_x (amplitude) and X_x (phase) on $\phi^{(2)}$. The pure space-time coupling is expressed by Φ_{xt} and X_{xt}.

Consider that the chirp introduced by the pulse shaper optimally compresses the pulse. With Δx=2mm (half-width at 1/e), v=0.15mm/ps, $\Delta\Omega$=25ps^{-1} (half-width at 1/e), $\phi_{in}^{(2)}$=160000fs^2, the pulse is stretched to 1ps with a Fourier limit of 20fs (half-width at 1/e). The optimal chirp compensation is $\phi^{(2)}$=-160000fs^2. The optimally compressed pulse half-width at 1/e is then given by $\Delta t=1/4\sqrt{\Phi_t}$=22.6fs. The 10% error is due to the decrease of Φ_t when $\phi^{(2)}$ increases. These values are extreme and in most of the cases, the introduced chirp is small enough not to impact the recompression. On the spatial characteristics the modifications are small compared to the beam size, the output beam size is Δx_p=1.998mm compared to Δx=2mm at the input.

To decrease the effect of this coupling, the ratio $v/\Delta x$ has to be kept small compare to the value of $\phi^{(2)}$, i.e. large input beams and highly dispersive gratings (p>600lines/mm).

As shown by Wefers [1996], it cannot by removed by a double pass configuration except for pure amplitude shaping. Despite its relatively small incidence on the output beam, this coupling can be very important when focusing the shaped pulse as shown by Sussman [2008] and Tanabe [2005].

To further analyze this pulse shaping technology, the mask has to be defined. The different technologies of spatial modulators are acousto-optic modulators (AOM) [Warren (1997)], Liquid Crystals Spatial Light Modulator diffraction-based approach [Vaughan (2005)], and Liquid Crystals Spatial Light Modulator. In the following, the mask used is a double Liquid Crystal Spatial Light Modulators (LC SLM) as described in Wefers (1995). The arbitrary filter is the combination of two LC SLM's whose LC's differ in alignment by 90 deg. This would produce independent retardances for orthogonal polarizations. The LC's for the two masks are respectiveley aligned at –45 and +45deg from the x axis, the incident light were polarized along the x axis, and the two LC SLM's are followed by a polarizer aligned along the x axis, the filter in this case for pixel n is given by

$$B_n = \exp\left\{i\left[\Delta\phi^{(1)} + \Delta\phi^{(2)}\right]/2\right\}\cos\left\{\left[\Delta\phi^{(1)} - \Delta\phi^{(2)}\right]/2\right\} = A_n e^{i\phi_n}, \tag{37}$$

where the dependence on the voltage for pixel n $\Delta\phi^{(i)}$ [$V_n^{(i)}$] is implicitly included. In this case neither mask acts alone as a phase or amplitude mask, but the two in combination are capable of independent attenuation and retardance. Furthermore, as the respective LC SLM's act on orthogonal polarizations, light filtered by one mask is unaffected by the second mask. As shown by Wefers and Nelson, this eliminates multiple-diffraction effects of the two masks.

As discussed previously, spatially large input pulses reduce the space-time coupling effect. Each dispersed frequency component incident upon the mask has a finite spot size associated with it. However, this blurs the discrete features of the mask, the incident frequency components should be focused to a spot size comparable with or less than the pixel width. If the spot size is too small, replica waverforms that arise from discrete Fourier sampling will be unavoidable. On the other hand, if the spot size is too big, the blurring of the mask will give rise to substantial diffraction effects. As the spatial profile of a wavelength on the mask is the Fourier transform of the spatial profile on the grating. Minimizing the space-time coupling by using spatially large input pulses, discrete Fourier sampling and pulse replica cannot be avoid as the following analysis (suggested by Vaughan [2005] and Monmayrant[2005]) will show.

The modulating function m(x) is simply the convolution of the spatial profile S(x) of a given spectral component with the phase and amplitude modulation applied by the LC SLM,

$$m(x) = S(x) \otimes \sum_{n=-N/2}^{N/2} squ\left(\frac{x - x_n}{\delta x}\right) A_n \exp(i\phi_n), \tag{38}$$

where x_n is the position of the nth pixel, A_n and ϕ_n are the amplitude and phase modulation applied by the nth pixel ($A_n\exp(i\phi_n)=B_n$), δx is the separation of adjacent pixels, and the top-hat function squ(x) is defined as

$$squ(x) = \begin{cases} 1 & |x| \le 1/2 \\ 0 & |x| > 1/2 \end{cases}. \tag{39}$$

The spatial profile S(x) of a given spectral component is directly the Fourier transform of the input spatial profile as

$$S(x) = TF\left[E_{in}(x_{in})\right]_{x=2\pi x_{in}/\lambda f \beta}, \tag{40}$$

where f is the focal length,
Here, the grating dispersion is assumed to be linear by

$$x(\omega) = \alpha(\omega - \omega_0), \text{where } \alpha = \frac{2\pi cf}{\omega_0^2 p \cos\theta_d(\omega_0)}. \tag{41}$$

Thus the position of the nth pixel x_n corresponds to a frequency $\Omega_n=n\delta\Omega$, where the frequency Ω_n of the nth pixel is defined relative to the center frequency ω_0 by $\Omega_n=\omega_n-\omega_0$, and where $\delta\Omega$ is the frequency separation of adjacent pixels corresponding to δx:

$$\delta\Omega = \frac{\delta x \omega_0^2 p \cos\theta_d(\omega_0)}{2\pi cf}. \tag{42}$$

Assuming also that the spatial field profile of a given spectral component is a Gaussian function $S(x)=\exp(-x^2/\Delta x^2)$, the modulation function may be written as

$$m(\Omega) = \exp\left(\frac{-\Omega^2}{\Delta\Omega_x^{\,2}}\right) \otimes \sum_{n=-N/2}^{N/2} squ\left(\frac{\Omega - \Omega_n}{\delta\Omega}\right) A_n \exp(i\phi_n). \tag{43}$$

Here the width of the spatial Gaussian function has been expressed in terms of $\Delta\Omega_x$, the spectral resolution of the grating-lens pair, where $\Delta\Omega_x=\Delta x\delta\Omega/\delta x$. The spot size Δx (measured as half-width at 1/e of the intensity maximum, assuming a Gaussian input beam profile) is dependent upon the input beam diameter D (half-width at 1/e), the focal length f and the angles of incidence and diffraction of the grating according to

$$\Delta x = \left(\left(\lambda_0 f \cos(\theta_i)\right)/\left(\pi D \cos(\theta_d)\right)\right). \tag{44}$$

The width of the Gaussian function expressed in frequency is

$$\Delta\Omega_x = \left(\omega_0 p \cos\left(\theta_i\right)\right)/\left(\pi D\right). \tag{45}$$

If we assume that the input pulse is a temporal delta function, $E_{in}(\Omega)=1$. The output field corresponds to the response function of the filter and its Fourier transform yields an expression of the impulse response function:

$$E_{out}(t) = h(t) \propto \exp\left(-\Delta\Omega_x{}^2 t^2/4\right)\sin c\left(\delta\Omega t/2\right)\sum_{n=-N/2}^{N/2} A_n \exp\left(i\left(\Omega_n t + \phi_n\right)\right). \tag{46}$$

The summation term describes the basic properties of the output pulse, such as would be obtained by modulating amplitude and/or phase of the input pulse at the point Ω_n with a grating-lens apparatus that has perfect spectral resolution. The sinc term is the Fourier transformation of the top-hat pixel shape, where the width of the sinc function is inversely proportional to the pixel separation δx, or equivalently, δΩ. The Gaussian term results from the finite spectral resolution of the grating lens-pair, where the width of the Gaussian function is inversely proportional to the spectral resolution $\Delta\Omega_x$. Collectively, the product of the Gaussian and sinc terms is known as the time window. Therefore to increase the time window, both the frequency separation of adjacent pixel δΩ and the spectral resolution $\Delta\Omega_x$ have to be increased.

The expression of the impulse response function (eq.46) contains a summed term that is a complex Fourier series. A property of Fourier series (with evenly-spaced frequency samples) is that they repeat themselves with a period given by the reciprocal of the frequency increment $T_0=1/\delta\Omega$. These pulses repetitions, refered as sampling replica, are a cause of concern since they can degrade the quality of the desired output waveform.

While eq. 46 provides a compact and useful analytical result, it considers only the LC SLM with perfect pixels and spatial spot size. It neglects some important limitations of these devices. First, the pixels of the LC SLM are not perfectly sharp, and there are gap regions between the pixels whose properties are somewhat intermediate between those of the adjacent pixels. Second, LC SLMs typically have a phase range that is only slightly in excess of 2π. Fortunately since phases that differ by 2π are mathematically equivalent, the phase modulation may be applied modulo 2π. Thus, whenever the phase would otherwise exceed integer multiples of 2π, it is "wrapped" back to be within the range of 0-2π. Although smoothing of the pixelated phase and/or amplitude pattern might in general sound desirable, when it is combined with the phase-wraps, distortions in the spectral phase and/or amplitude modulation are introduced at phase-wrap points. Third, while the pixels are evenly distributed in space, the frequency components of the dispersed spectrum are not. This nonlinear mapping of pixel number to frequency makes difficult the determination of an exact analytical expression for m(Ω).

The contribution of the gaps has been taken into account in the litterature (Wefers [1995], Montmayrant[2005]) as a constant complex amplitude. This analysis supposes that the gap region does not depend upon the neighbour pixels. As the filter in each gap is assumed to be the same, the gaps simply reproduce the single input pulse at time zero with a reduced complex amplitude given by $(1\text{-}r)B_g$ where r is the ratio of the pixel width (rδx) by the pixel pitch δx and B_g its complex response. The expression for m(x) including the gaps is

$$m(x) = S(x) \otimes \sum_{n=-N/2}^{N/2}\left[\left(squ\left(\left(x-x_n\right)/r\delta x\right)A_n \exp\left(i\phi_n\right)\right) + \left(squ\left(\left(x-x_n+\delta x/2\right)\Big/\left(\left(1-r\right)\delta x\right)\right)B_g\right)\right]. \tag{47}$$

With the approximation of linear spectral dispersion, the filter response function can be expressed as:

$$h(t) \propto E_{in}\left((p\omega_0 \cos\theta_i/2\pi)t\right)\left\{\left[r\,\mathrm{sinc}\left(r\,\delta\Omega t/2\right)\sum_{n=-\infty}^{\infty}A_n e^{i(\Omega_n t+\phi_n)}\right]+\left[(1-r)\mathrm{sinc}\left((1-r)\delta\Omega t/2\right)\sum_{n=-\infty}^{\infty}B_g e^{i\Omega_n t}\right]\right\}. \quad (48)$$

The time extent of the contribution of the gap is a lot longer than the pixel one. The theoretical ratio in intensity is $(r/(1\text{-}r))^2$ in the order of thousand for up-to-date LC SLM. But the experimental ratio is about 40 to 100. This order of magnitude is due to the hypthesis that the gap region is the same and that the pixel edges are perfectly sharp. The smoothing of the phase between pixels has to be considered.

The smoothing function has been first introduced by Vaughan and al. but without explicit expression, and on a phase mask only. In fact no simple analytical model can reproduce this effect. It will be introduce in the simulation part.

The phase wraps used to extend the phase modulation of the LC SLM above its limited excursion of 2π by applying a phase that is "wrapped"back into $0\text{-}2\pi$ as

$$\phi_{applied,n} = \mathrm{mod}_{2\pi}\left[\phi_{desired,n}\right]. \quad (49)$$

Due to the mathematical equivalence of phase values that differ by integer multiples of 2π, there are an infinite number of ways to "unwrap"the applied phase. Sampling replica pulses constitute an important class of these equivalent phase functions, and their phase as a function of pixel, $\phi_{replica,n}$, may be described by

$$\phi_{replica,n} = \phi_{applied,n} + 2\pi Rn, \quad (50)$$

where R is the sampling replica order and may be any non zero integer (0 corresponds to the desired pulse). In the case of linear spectral dispersion, $\phi_{replica,n}$ for different values of R differ by a linear spectral phase $2\pi R\omega/\delta\Omega$, which corresponds to a temporal shift of $R/\delta\Omega$. This is another explanation of the sampling replica that are temporally separated by $1/\delta\Omega$. In the case of a non linear spectral dispersion, the different replica phases do not differ by a linear spectral phase but rather by a non linear one. The quadratic term will introduce a second order spectral phase (chirp) linearly depending on the replica number R. A very explicit illustration is given by Vaughan and al.(2006), but no analytical expression could be given for the non linear dispersion.

Finally, the modulation function can be expressed analytically as

$$m(\Omega) = squ\left[\Omega/N\delta\Omega\right]\left\{S(\Omega)\otimes comb\left[\Omega/\delta\Omega\right]\left[squ\left(\Omega/r\delta\Omega\right)H(\Omega)+squ\left(\left(\Omega+\delta\Omega/2\right)\Big/\left((1-r)\delta\Omega\right)\right)B_g\right]\right\}, \quad (51)$$

where $comb\left[\Omega\right]=\sum_{n=-\infty}^{\infty}\delta\left(\Omega-n\right)$, N is the number of pixels, H(Ω) is the desired transfer function. This function combines the pixelization, the gap effect, the input beam spatial dimension, the limited number of pixel. The impulse response function is then given by

$$M(t) \propto sinc\left[N\,\delta\Omega t/2\right]\otimes\left[E_{in}\left(\left(\frac{p\omega_0\cos\theta_i}{2\pi}\right)t\right)\left\{\begin{matrix}\left(r\sin c\left(r\,\delta\Omega t/2\right)\left(comb\left[\delta\Omega t\right]\otimes h(t)\right)\right)+\\ r\sin c\left(\pi(1-r)\delta\Omega t/2\right)\left(comb\left[\delta\Omega t\right]\otimes B_g\right)\end{matrix}\right\}\right]. \quad (52)$$

where N is the pixels number, $\delta\Omega$ is the frequency extent of a the pixel pitch, S(x) is the spatial profile of the input pulse, r the ratio between the pixel size and the pixel pitch, h(t) the ideal impulse response function and B_g the gap complex transmission.
The figure 3 illustrates the different contributions of this model on the output temporal intensity.

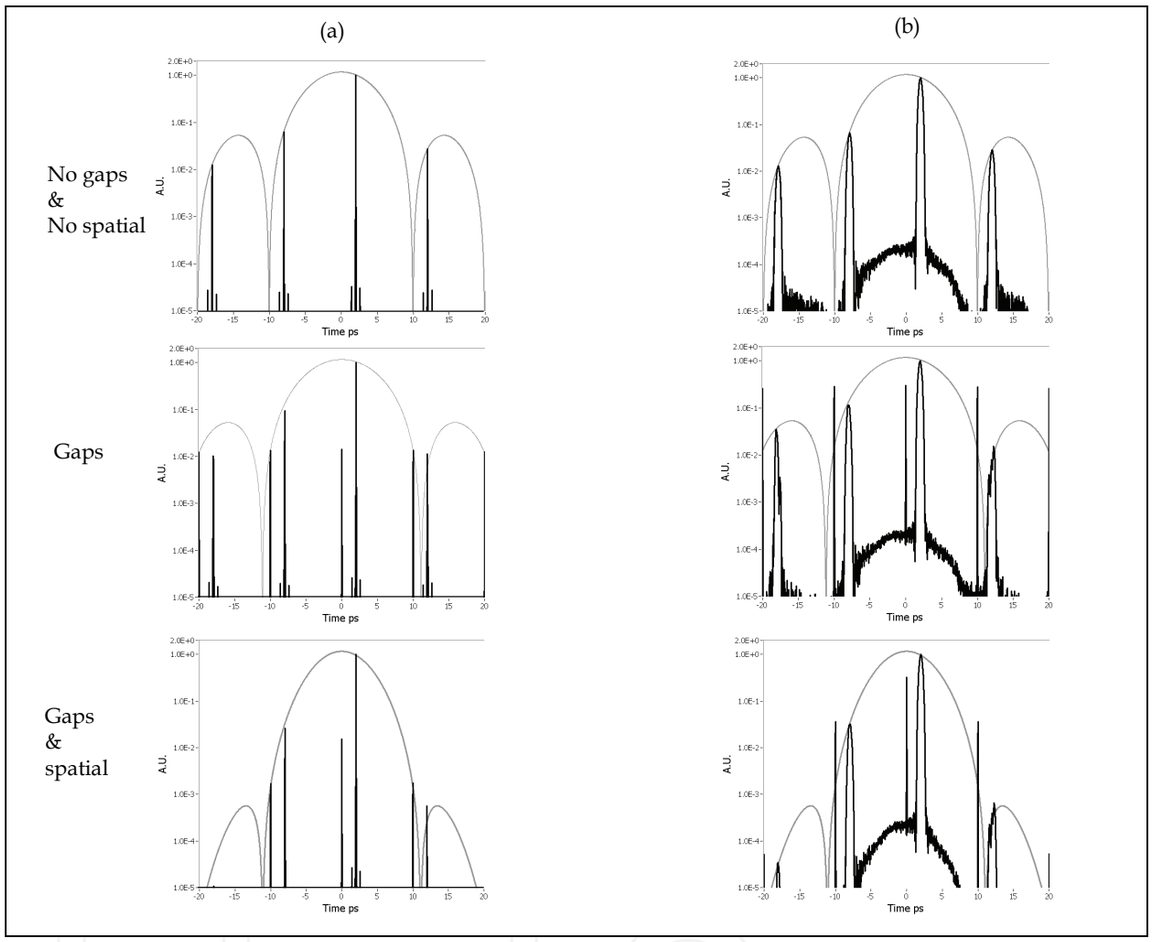

Fig. 3. output temporal intensity examples in logarithmic scale for a 4-f pulse shaper (f=220mm,2000lines/mm, δx=100μm, r=0.9, D=1.7mm half-width at 1/e, B_g=1) with (a) a delay 2000fs, (b) adding a chirp 4000fs² to the delay. The first row does not include contribution of gaps and spatial filtering, second row includes gaps contribution, third row gaps and spatial input beam profile contribution. The black line is the output waveform, the grey line the envelope of the filter response pulse shaper pixels.

Other contributions can only be numerically simulated as the non linear dispersion, the smoothing effect, the spatio-temporal coupling.
The pulse replicas can be filtered out as the spatio-temporal coupling by using a spatial filter at the output (cf Fig.5). This filtering effect is only efficient if the filter select the lowest Hermite-Gaussian mode as shown by Thurston and al. (1986). Regenerative amplifiers or monomode optical fibers are good fundamental Hermite-Gaussian mode filters. A simple iris cannot be considered as such a filter as shown by Wefers (1995). With perfect filtering, the filter modulation becomes

$$m_{filtered}(t) \propto Filter(t) \cdot m(t) \propto sinc\left[N\delta\Omega t/2\right] \otimes \left\{rh(t) + (1-r)B_g\right\}. \quad (53)$$

The filter function Filter(t) introduced by the spatial filtering decreases the overall efficiency and does not filter out the contribution of the gaps. It can be estimated as applying another enveloppe on the time profile with a restricted area limiting the time window. The contribution of the filters response has to be taken into account for exact pulse shaping.

4.1.2 4-f pulse shapers numerical simulations

4-f pulse shapers are commonly used with a simple iris aperture filtering directly at the output before the experiment. As seen in the previous part, the filter response can be affected by limitations of the 4-f apparatus (spatio-temporal coupling, non linear dispersion) and of the LC SLMs (smoothing) that cannot be expressed analytically. Complex input pulse and pulse shaping as multiple pulses or square pulses can only be simulted numerically. This part gives an adavnced numerical models combining models used in the litterature (Wefers [1995], Vaughan [2005], Monmayrant [2005], Sussman [2008], Tanabe [2002], Tanabe [2005]).

The effects of pulse propagation through a pulse shaper have been carefully detailed by Danailov [1989] and Wefers [1995]. As Tanabe (2005) and Sussman (2008), the propagation is simulated by a Fresnel propagation as:

$$\tilde{E}(k_x, \omega, z) = e^{-i\pi k_x^2 (z-z_0)c/\omega} \tilde{E}(k_x, \omega, z_0), \quad (54)$$

where $\tilde{E}(k_x, \omega, z)$ is the spatial Fourier transform of the electric field, $U_{Fresnel}(k_x) = e^{-i\pi k_x^2 (z-z_0)c/\omega}$ is the Fresnel propagator. The field will be simulated at a focal plane as oftenly used experimentally.

For the shaper in Fig.4, there are 17 different steps from input beam to focal field, as enumerated below.

1. An input beam E(x,t,0) is propagated from its origin to the diaphragm aperture of the pulse shaper by Fresnel propagation.
2. An iris aperture spatially of diameter D_{iris} filters the beam:
   $E(x,t,z) \rightarrow \mathrm{Rect}(x/D_{iris}) E(x,t,z)$.
3. The beam is propagated form the iris to the input grating by Fresnel propagation.
4. The beam is dispersed by the input grating by applying Martinez:
   $E(x,\Omega,z) \rightarrow \sqrt{\beta} e^{2i\pi\gamma\Omega x} E(\beta x,\Omega,)$
5. The beam is Fresnel propagated a distance f.
6. A perfect thin lens of focal length f introduces a quadratic spatial phase: $E(x,\Omega,z) \rightarrow E(x,\Omega,z) e^{-i\pi\Omega f x^2/2c}$.
7. The beam is Fresnel propagated a distance f.
8. The spatial mask is applied via multiplication:
   $E(x,\Omega,z) \rightarrow E(x,\Omega,z) m(x)$
9. The beam is Fresnel propagated a distance f.
10. A perfect thin lens of focal length f introduces a quadratic spatial phase : $E(x,\Omega,z) \rightarrow E(x,\Omega,z) e^{-i\pi\Omega f x^2/2c}$.

11. The beam is Fresnel propagated a distance f.
12. The second grating is applied in the inverted geometry by applying Martinez: $E(x,\Omega,z) \to \left(1/\sqrt{\beta}\right) e^{2i\pi\gamma\Omega x} E(-x/\beta,\Omega,z)$.
13. The beam is Fresnel propagated from the grating to the output iris.
14. The beam is spatially filtered by the iris: $E(x,t,z) \to \mathrm{Rect}\left(x/D_{iris}\right) E(x,t,z)$.
15. The beam is Fresnel propagated a distance L
16. A thin lens of focal length f_L is applied: $E(x,\Omega,z) \to E(x,\Omega,z) e^{-i\pi\Omega f_L x^2/2c}$
17. The beam is propagated to the focal plane.

The spatio-temporal coupling is directly include in these steps. All the other effects can be introduced directly on the mask and grating functions.
The non linear dispersion is estimated through a modification of the mask by introducing:

$$\Omega(x) = ax + bx^2 + O(x^2), \tag{55}$$

where $a = p\omega_0{}^2 \cos\theta_d / 2\pi cf$, $b = p^2\omega_0{}^3 \left(\cos\theta_d\right)^2 / 8\left(\pi cf\right)^2$. This contribution has to be corrected for the main pulse but still remains for the replica.
The pixelization is introduced on the mask by

$$m(x) = \sum_{n=-N/2}^{N/2-1} rect\left[\frac{x - x_n}{\delta x}\right] A_n e^{i\phi_n}. \tag{56}$$

The smoothed-out pixel regions may cause an entirely different class of output waveform distortions from the pixel gap as mentionned by Vaughan and al. (2006). Although the exact nature of the smooth pixel boundaries is expected to be highly dependent upon the specific device that is being considered, it has been approximated by convolving a spatial response function L(x) with an idealized phase modulation function that would result in the case of sharply defined pixel and gap regions (Vaughan [2005]). But no explicit smoothing function has been given in the litterature. Moreover this approximation stands only for a phase only pulse shaper. The exact analysis of a phase step between two adjacent pixels is very complex. A simple model can consider that the phase introduced by a LC SLM is given by

$$\phi(\lambda,V) = \frac{2\pi\Delta n(\lambda,V) e_{LC}}{\lambda} = e^{P(V)} + C. \tag{57}$$

Despite the sharp edges of the pixel, a relaxation process occurs in the Liquid Crystal material whose anisotropy is very strong ($\varepsilon_{//} \approx 5\ \varepsilon_{\perp}$) [Khoo (1993)]. For an up-to-date LC SLM, the pixel pitch is 100µm and the gap 2µm, the thickness is about 10µm. Without taking into account the anisotropy, the smoothing is about 1/20 of the pixel pitch independantly of the gap size. With the anisotropy, the smoothing covers more than half the pixel. A rather good smoothing function is a Lorentzian:

$$L(x) = \frac{\Gamma/2\pi}{x^2 + \left(\Gamma/2\right)^2}, \tag{58}$$

where Γ is the width.

With the relaxation, the small gaps completely disappear. This smoothing has to be done on the potential of the LC SLM directly. So from the desired phase modulation on both LC SLMs, the potential is calculated, smoothed by the Lorentzian, and discretized according to to the voltage resolution of the device.

So the estimation of the mask modulation can include the non-linear dispersion, the pixelization and pixels smoothing by applying the following algorithm:

1. From a regular array of points in the space domain of the mask x_n, estimation of the corresponding frequencies with the non linear dispersion : Ω_n.
2. Determination of the amplitude and phase of the ideal mask on these frequencies: $A_n(\Omega_n)$ and $\phi_n(\Omega_n)$.
3. Determination of the frequencies relative to each pixel: Ω_k^{pixel}.
4. Pixelization of the phase and amplitude by applying the same phase and amplitude over a pixel i.e. for $\Omega_n \in [\Omega_k^{pixel}, \Omega_{k+1}^{pixel}]$.
5. Pixels smoothing by:
   a. Estimation of the phases on the two LC SLMs:
      $\Delta\phi^{(1)} = \left(a\cos\left(A_n\right) + \phi_n\right)/2, \Delta\phi^{(2)} = \left(a\cos\left(A_n\right) - \phi_n\right)/2$.
   b. Determination of the voltage on the pixels by inverting eq.57:
      $V_1 = f^{-1}\left(\Delta\phi^{(1)}\right), V_2 = f^{-1}\left(\Delta\phi^{(2)}\right)$.
   c. Smoothing of this voltages by convolving with the Lorentzian function (eq.58):
      $V_{i,smoothed}\left(\Omega\right) = L\left(\Omega\right) \otimes V_i\left(\Omega\right)$.
   d. Calculation of the two LC SLMs phases: $\Delta\phi^{(i)}_{smoothed} = f\left(V_{i,smoothed}\right)$.
   e. Calculation of the mask modulation from eq.37.

The numeric propagation of pulses is efficiently achieved using the fast Fourier transform (FFT) and its inverse (IFFT), for transforming between space to frequency and time to frequency. Care should be taken to assure that the sampling is done correctly. Propagating through large distances or studying the intensity close to the focal point requires resampling the spatial grid. The spatio-temporal complete simulation requires a bidimensionnal grid in space and time restricting the resolution in time. Specific study of sampling replica, pixels smoothing effects and gaps should be done with a simplified model without the space-time coupling. For example, for a pulse shaper with 640 pixels and pixel gaps about 3% of the pixel pitch, the number of sampling points (>10000) is too high for this bidimensionnal simulation. The simplification consists in directly multiplying the input pulse by the mask function in the frequency domain as

$$E_{out}\left(\Omega\right) = E_{in}\left(\Omega\right)M(\Omega) \propto E_{in}\left(\Omega\right)TF\left[E_{xin}\left(t/v\right)TF^{-1}\left[M\left(\Omega\right)\right]\right], \tag{59}$$

where $M(\Omega)$ is calculated by the algorithm described just beneath.

These models are in quantitative agreement with experimental published results. The different contributions (pixelization, non-linear dispersion, pixel gaps and pixels smoothing) are illustrated on the figure 4 below on a 100fs Fourier transform pulse at 800nm delayed by –2ps, or stretched by a $7.10^5 fs^2$ chirp, with a pulse shaper using two LC SLMs 0f 640 pixels (pixel pitch=100μm, pixel size=0.97), a focal length of 200mm and a 2000lines/mm grating with equal input and output angles. The input beam diameter is 2.3mm gaussian shape.

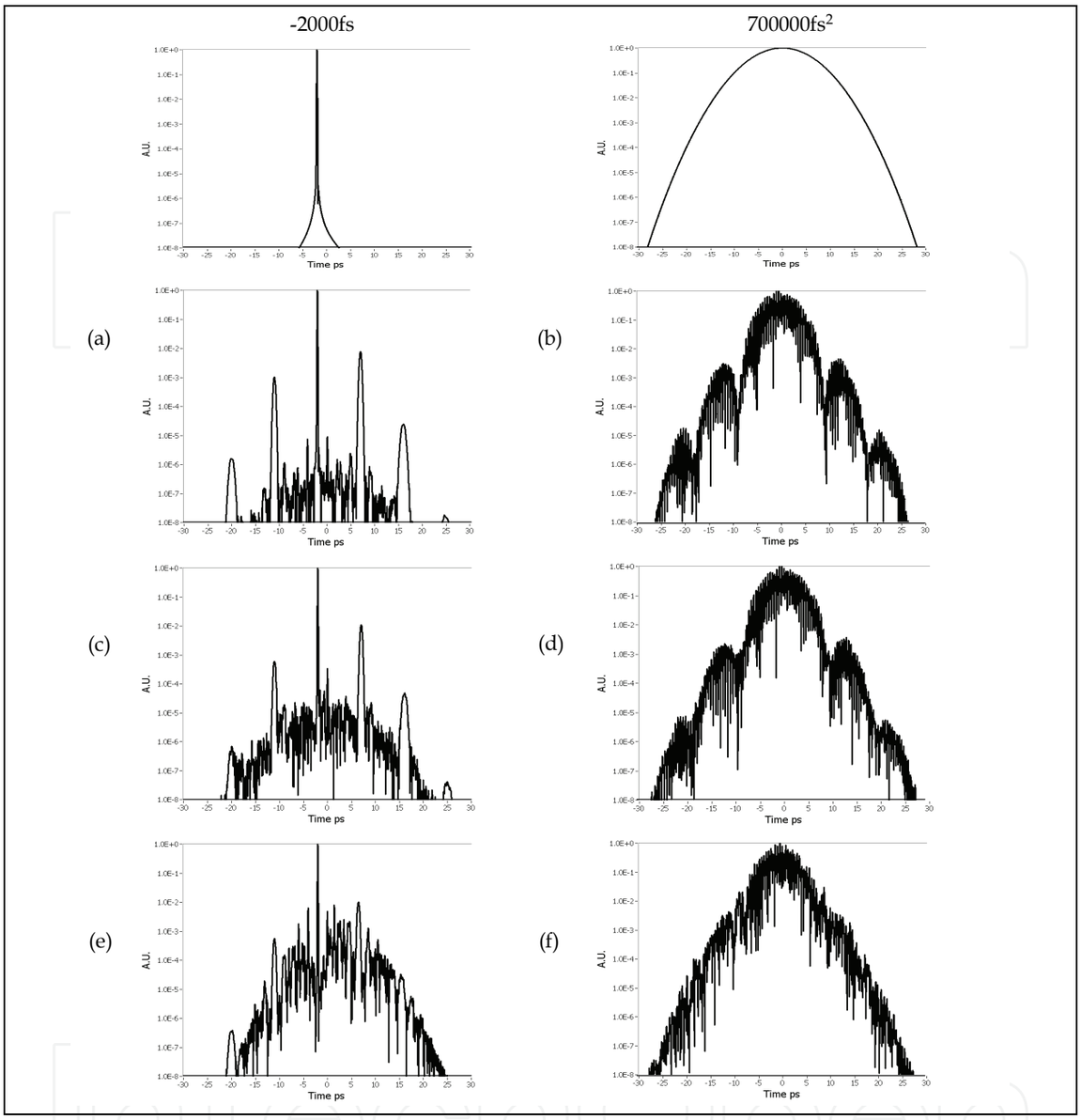

Fig. 4. Contributions on pulses with a –2ps delay or a 0.7ps² chirp of (a),(b) non-linear dispersion, (c),(d) pixel gaps, (e),(f) pixels smoothing.

4.1.3 Conclusions on 4-f pulse shapers

This pulse shaper technology based on the coupling between space and time in a 4f-zero dispersion line apparatus allows complex pulse shaping over a large range of pulse characteristics. Its optical set-up allows to adapt the performances of the pulse shaper. Despite its relative simple concept, its optimization requires a trade-off between parameters and side effects.

The parameters are: p the grating pitch, f the focal length, θ_i the incidence angle, θ_d the diffracted angle, δx the pixel pitch, N the number of pixels and D the input beam diameter.

The relevant characteristics are:

- The spectral bandwidth: $\Delta\Omega_M = \left(\omega_0^2 p\cos\theta_d / 2\pi c\right)\arctan\left(N\,\delta x / f\right)$,
- spectral resolution or initial time window : $\delta\Omega = 1/\delta T = \delta x \omega_0^2 p\cos\theta_d / 2\pi c f$,
- spatio-temporal slope : $v = -\gamma/\beta = 2\pi / \omega_0 p\cos\theta_i$,
- real time window (spatial filtering) : $\Delta T = D / v$,
- Rayleigh length at the mask: $z_R = \lambda f^2 / \pi D^2$.

The Rayleigh length has to be larger than the two LC SLMs mask thickness which is typically about 1mm.
To decrease the spatio-temporal coupling, v/D has to be minimized, but this also reduces the time window. Thus a trade-off between the side-effects of the spatio-temporal coupling and the required time window and the pulse replica has to be done.
As mentionned by Wefers (1995), Monmayrant (2005) and Tanabe (2002), the pixel gaps and some other effects can be compensated for by iterative algorithms. As the models are not precise enough, this compensation has to be done experimentally (Tanabe).
The effects of misalignement and tolerances of the optical set-up is beyond the scope of this chapter but can be very significant on the output waveform as shown by Wefers (1995), Tanabe (2002).

4.2 Acousto-optic programmable dispersive filter

The second pulse shaping technology has been invented by Pierre Tournois in 1997 (Tournois (1997)). The basic idea is to make a programmable Bragg grating or chirped mirror. Through an acousto-optic longitudinal Bragg cell, the acousto-optic diffraction directly transfers the amplitude and phase modulation of the acoustic wave onto the optical diffracted beam.
A schematic of the AOPDF is shown on fig.5. An acoustic wave is launched in an acousto-optic birefringent crystal by a transducer excited by a temporal RF signal. The acoustic wave propagates with a velocity V along the z-axis of the crystal and hence reproduces spatially the temporal shape of the RF signal. Two optical modes can be coupled efficiently by acousto-optic interaction in the case of phase matching. If there is locally only one spatial frequency in the acoustic grating , then only one optical frequency can be diffracted at a position z. The incident optical short pulse is initially polarized onto the fast axis polarization of the birefringent crystal. Every optical frequency ω travels a certain distance before it encounters a phase matched spatial frequency in the acoustic grating. At this position z(ω), part of the energy is diffracted onto the slow axis polarization. The pulse leaving the device onto the extraordinary polarization will be made up all the spectral components that have been diffracted at various positions. Since the velocities of the two polarizations are different, each optical frequencies will see a different time delay τ(ω) given by:

$$\tau(\omega) = \frac{z(\omega)}{v_{g1}} + \frac{L - z(\omega)}{v_{g2}}, \tag{60}$$

where L is the crystal length, v_{g1} and v_{g2} are the group velocities of ordinary and extraordianry modes respectively.

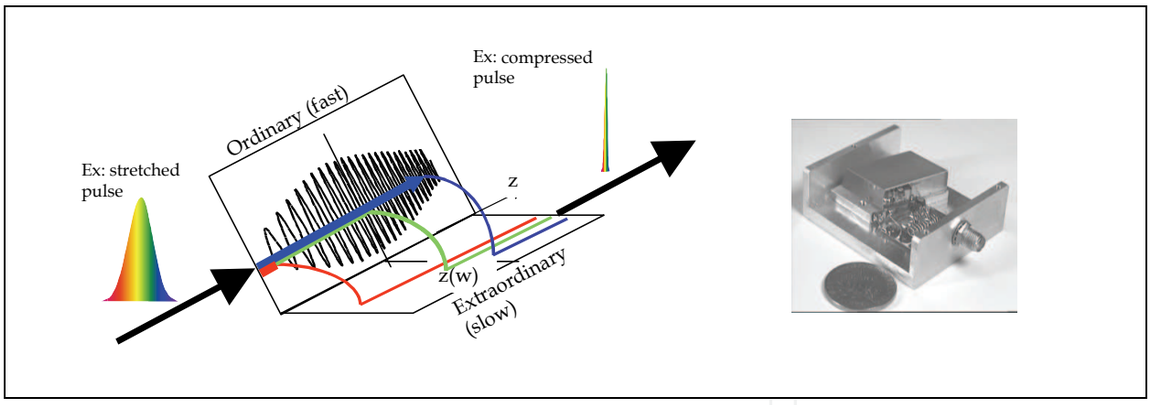

Fig. 5. Schematic of the AOPDF.

The amplitude of the output pulse, or diffraction efficiency, is controlled by the acoustic power at position z(ω). The optical output $E_{out}(t)$ of the AOPDF is a function of the optical input $E_{in}(t)$ and of the acoustic signal S(t). More precisely, it has been shown (Tournois (1997)), for low value of acoustic power density, to be proportionnal to the convolution of the optical input and of the scaled acoustic signal:

$$E_{out}(t) \propto E_{in}(t) \otimes S(t/\alpha) \Leftrightarrow E_{out}(\omega) \propto E_{in}(\omega) S(\alpha\omega), \tag{61}$$

where the scaling factor α is the ratio of the acoustic frequency to the optic frequency.
In this formulation, the AOPDF is exactly a linear filter whose filter response is S(αω). Thus by generating the proper function, one can achieve any arbitrary convolution with a temporal resolution given by the inverse of the available filter bandwidth.
This physical discussion qualitatively explains the principle of the AOPDF. A more detailed analysis is given in the following part based on a first order theory of operation, and second order influence will then be estimated.

4.2.1 First order theory of the AOPDF

The acousto-optic crystal considered in this part is Paratellurite TeO_2. The propagation directions of the optical and acoustical waves are in the P-plane which contains the [110] and [001] axis of the crystal. The acoustic wave vector K makes an angle θ_a with the [110] axis. The polarization of the acoustic wave is transverse, perpendicular to the P-plane, along the [/110] axis. Because of the strong elastic anisotropy of the crystal, the K vector direction and the direction of the Poynting vector are not collinear. The acoustic Poynting vector makes an angle β_a with the [110] axis. When one sends an incident ordinary optical wave polarized along the [/110] direction with a vector k_0 which makes an angle θ_0 with the [110] axis, it interacts with the acoustic wave. An extraordinary optical wave polarized in the P-plane with a wave vector k_d is diffracted with an angle θ_d relative to the [110] axis. To maximize the interaction length for a given crystal length, and hence to decrease the necessary acoustic power, the incident ordinary beam is aligned with the Poynting vector of the acoustic beam, i.e. $\beta_a=\theta_0$. Figure 10 shows the k-vector geometry related to the acoustical and optical slowness curves. V_{110} and V_{001} are the phase velocities of the acoustic shear waves along the [110] axis and along the [001] axis respectively. n_o and n_e are the ordinary and extraordinary indices on the [110] axis and n_d is the extraordinary index associated with the diffracted beam direction at angle θ_d.

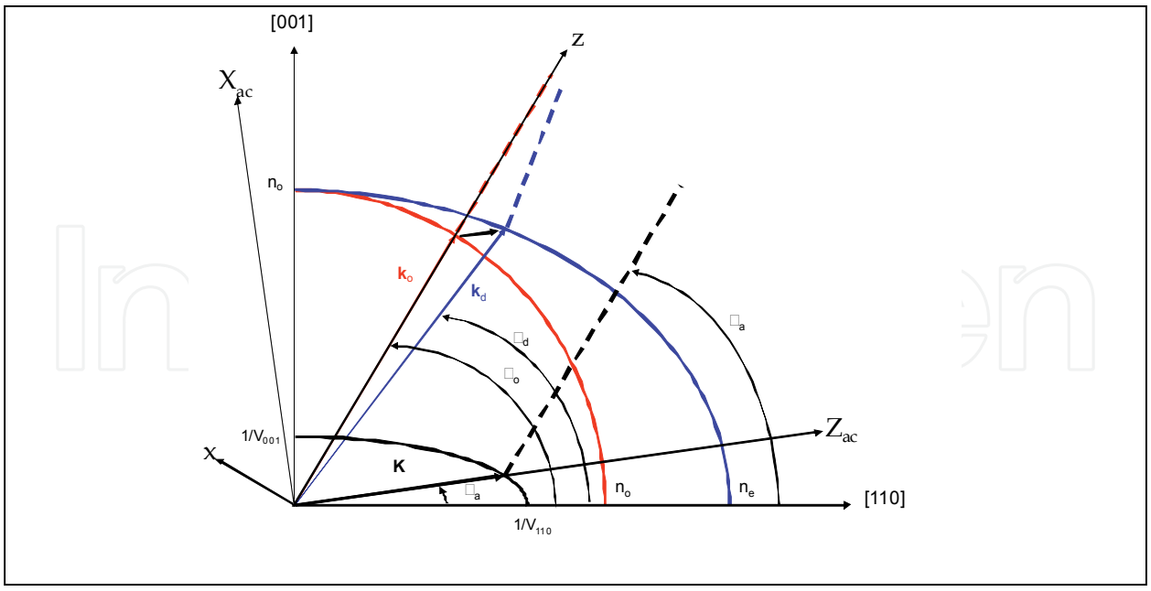

Fig. 6. Acoustic and optic slowness curves and k-vector diagram

The optical anisotropy $\Delta n=(n_e-n_o)$ being generally small as compared to n_o, the following relations can be obtained to first order in $\Delta n/n_o$:

$$\delta n = n_d - n_o = \Delta n.\cos^2\theta_0\,, \tag{62}$$

$$V(\theta_a) = \sqrt{{V_{001}}^2 \sin^2\theta_a + {V_{110}}^2 \cos^2\theta_a}\,, \tag{63}$$

$$\theta_d - \theta_0 = -(\Delta n/n_0).\cos^2\theta_0.\tan(\theta_0-\theta_a)\,, \tag{64}$$

$$K = k_0(\Delta n/n_0).\left(\cos^2\theta_0/\cos(\theta_0-\theta_a)\right), \tag{65}$$

$$\alpha = \left(V(\theta_a)\Delta n/c\right).\left(\cos^2\theta_0/\cos(\theta_0-\theta_a)\right), \tag{66}$$

where c is the speed of light.

The single frequency solution of the coupled mode theory for plane waves (Yariv and Yeh) allows to relate the diffracted light intensity to the incident light intensity and to the acoustic power density P(αω) present in the interaction area by the formula:

$$I_d(\omega) = I_0(\omega)\left(P(\alpha\omega)/P_0\right)\frac{\pi^2}{4}\sin c^2\left[\frac{\pi}{2}\sqrt{\left(P(\alpha\omega)/P_0\right)+\left(\frac{\delta\varphi}{\pi}\right)^2}\right] \text{ with } P_0 = \frac{1}{2M_2}\left[\frac{\lambda}{L\cos(\theta_0-\theta_a)}\right]^2, \tag{67}$$

with δφ is an asynchronous factor proportional to the product of the departure δk from the phase matching condition and of the interaction length along the acoustic wave vector K:

$$\delta\varphi = \frac{\delta k}{\pi}L\cos(\theta_0-\theta_a) \approx \frac{\Delta n}{n_o}k_0 L\cos\theta_0\left[\frac{-\delta\omega}{\omega}+\delta\theta_0\left(2\tan\theta_0-\tan(\theta_0-\theta_a)\right)\right], \tag{68}$$

L being the interaction length along the optical wave vector k_0, λ the wavelength of the light in vacuum, ρ the density of TeO_2 crystal, p an elasto-optic coefficient, and M_2 the merit factor given by:

$$M_2 = \frac{n_o{}^3\left[n_d(\theta_d)\right]^3\left[p(\theta_0,\theta_a)\right]^2}{\rho\left[V(\theta_a)\right]^3} \text{ with } p(\theta_0,\theta_a) = -0.17\sin\theta_a\cos\theta_0 + 0.09\sin\theta_0\cos\theta_a. \quad (69)$$

From eq.67, with a perfect matching condition (δφ=0), complete diffraction of an optical frequency ω corresponds to an acoustic power density $P(\alpha\omega)=P_0$. As the interaction is longitudinal or quasi-collinear the efficiency of diffraction is excellent. P_0 is in the order of few mW/mm^2.

The spectral resolution and angular aperture are defined by the phase matching condition through the condition that the efficiency $\eta=I_d/I_0=0.5$ for $\delta\varphi=\pm 0.8$ when $P(\alpha\omega)=P_0$ as:

$$\left(\frac{\delta\lambda}{\lambda}\right)_{1/2} = \left(\frac{\delta\omega}{\omega}\right)_{1/2} = \frac{0.8}{\Delta n\cos^2\theta_0}\frac{\lambda}{L}, \quad (70)$$

$$(\delta\theta_0)_{1/2} = \left(\frac{\delta\lambda}{\lambda}\right)_{1/2}\frac{1}{\left[2\tan\theta_0 - \tan(\theta_0-\theta_a)\right]}. \quad (71)$$

By using conventionnal acousto-optic technology, diffraction efficiencies can be up to 50% over 100nm. If Δλ is the incident optical bandwidth, the number of programming points N and the estimation of the acoustic power density to maximally diffract the whole bandwidth will be:

$$N = \frac{\Delta\lambda}{(\delta\lambda)_{1/2}} = \frac{\Delta nL\cos^2\theta_0}{0.8}\frac{\Delta\lambda}{\lambda^2}, \quad (72)$$

$$P_N = NP_0 = \frac{1.25\Delta n\cos^2\theta_0}{2M_2\cos^2(\theta_0-\theta_a)}\frac{\Delta\lambda}{L}. \quad (73)$$

The different applications of the AOPDFs call for two different cut optimizations of the TeO_2 crystal. When the goal is to control the spectral phase and amplitude in the largest possible bandwidth, to obtain the shortest possible pulse, the diffraction efficiency has to be maximized and hence P_0 minimized (Wide Bandc cut). When the goal is to shape the input pulse width with the higher resolution, the optimization is a trade-off between the spectral resolution and the diffraction efficiency (High Resolution cut). The parameters for the Wide Band and High Resolution AOPDFs for λ=800nm are given in table 1.

Since Paratellurite crystals are dispersive, the acoustic to optic frequency ratio α depends on the wavelength through the spectral dispersion of optical anisotropy.

The dispersion becomes very large below λ=480nm. For limited bandwidth Δλ, the dispersion of the crystal can be compensated b y programming an acoustic wave inducing an inverse phase variation in the diffracted beam. This self-compensation is, however, limited by the maximum group delay variation given by:

AOPDFs name	L mm	θ_a deg	θ_0 deg	$\theta_d-\theta_0$ deg	α 10^{-7}	$n_o(\delta\theta_0)_{1/2}$ deg	P_0 MW/ mm²	$(\delta\lambda)_{1/2}$ nm	T ps	$\Delta\lambda$ (η=0.5 for 0.6W/mm²) nm	N
Wide Band 25 (WB25)	25	8	58.5	1.25	1.42	0.04	4.5	0.6	3.7	100	170
High Resolution 25 (HR25)	25	3.9	38.5	1.60	2.3	0.045	3.8	0.25	8.0	50	200
Wide Band 45 (WB45)	45	8	58.5	1.25	1.42	0.022	1.4	0.33	6.7	180	540
High Resolution 45 (HR45)	45	3.9	38.5	1.60	2.3	0.025	1.2	0.14	14.4	90	640

Table 1. Standard AOPDFs parameters.

$$\delta\tau_g = \tau_{gd} - \tau_{g0} = \left(n_{gd} - n_{g0}\right)\frac{L}{c} = \left(n_{gd} - n_{g0}\right)\cos^2\theta_0\frac{L}{c}. \tag{74}$$

More precisely, when the dispersion of the crystal is compensated by an adapted acoustic waveform, all the wavelength in the optical bandwidth $\Delta\lambda=\lambda_2-\lambda_1$ have to experience the same group delay time, i.e. the same group index $n_{g0}(\lambda_1)=n_{gd}(\lambda_2)$. The maximum bandwidth of self compensation depends upon the central wavelength and the crystal type (cf table 2).
If the bandwidth of operation is larger than this maximum bandwidth $\Delta\lambda$, it is necessary to use an outside compressor. The major component of the dispersion in TeO_2 is the second order. If this second order is externally compensated this leads to a new limit bandwidth $\Delta\lambda_1>\Delta\lambda$ associated to higher orders compensation.

Central lambda	650 nm	800 nm	1064 nm	1550 nm
$\Delta\lambda$ nm/ $\phi^{(2)}$ fs² / $\Delta\lambda_1$ nm WB 25	45 / 17300 / 300	70 / 12800 / 560	150/ 8900 / >600	500/ 5370 />1000
$\Delta\lambda$ nm/ $\phi^{(2)}$ fs² / $\Delta\lambda_1$ nm HR 25	130 / 17300 / >400	200 / 12800 / >800	420/ 8900 / >800	800/ 5370 />1000
$\Delta\lambda$ nm/ $\phi^{(2)}$ fs² / $\Delta\lambda_1$ nm WB 45	80 / 17300 / >400	125 / 23000 / 800	270/ 1600 / >800	900/ 9660 />1000
$\Delta\lambda$ nm/ $\phi^{(2)}$ fs² / $\Delta\lambda_1$ nm HR 45	230 / 17300 / >400	360 / 23000 / >800	725/ 1600 / >800	>1000/ 9660 />1000

Table 2. Self-compensation bandwidth $\Delta\lambda$, second order dispersion and higher order limited bandwidth $\Delta\lambda_1$.

4.2.2 Rigourous theory of the AOPDF

The first order theory is a good approximation despite strong hypothesis of acoustic and optic plane waves, acoustic and optic single frequencies. The validity of these two hypothesis is studied in the following parts.

4.2.2.1 From the single frequency to the multiple frequencies

The multi-frequencies general approach (Laude (2003)) is complex and not actually required for the simulation of the AOPDF (Oksenhendler (2004)). In the AOPDF crystal geometry, as

only one diffracted mode can exist, the coupled-wave equation can be simplified and expressed in a matrix notation such as:

$$\frac{\partial \hat{D}}{\partial z} = jM(z)\hat{D} \text{ where } M(z) = \begin{pmatrix} 0 & \kappa(z) \\ \kappa^*(z) & 0 \end{pmatrix},\ \hat{D}(z) = \begin{pmatrix} D_0 \\ D_1 \end{pmatrix} \tag{75}$$

with $\kappa(z) = -\frac{j}{4} k_0 \sqrt{n_0^3}\sqrt{n_d^3} L \int A(\omega_{ac}) e^{-j\psi(\omega_{ac})} \left(e^{j(\mathbf{k}_{0z} - \mathbf{k}_{1z} + \mathbf{K}(\omega_{ac}))z} \right) d\omega_{ac}$,

where the index 0,1 corresponds respectively to the incident and diffracted beam, D is the electric displacement vector, A the acoustic complex amplitude.
This equation can be solved independently of the number of acoustic frequencies considered. The solutions are:

$$\begin{pmatrix} D_0(L) \\ D_1(L) \end{pmatrix} = \exp\left(j \int_0^L M(z)\, dz \right) \begin{pmatrix} 1 \\ 0 \end{pmatrix}. \tag{76}$$

The difference with the first order theory is within 1% on the spectral amplitude. The spectral phase is conserved even in the saturated or over saturated regime because it comes directly from the phase matching condition (fig.6).

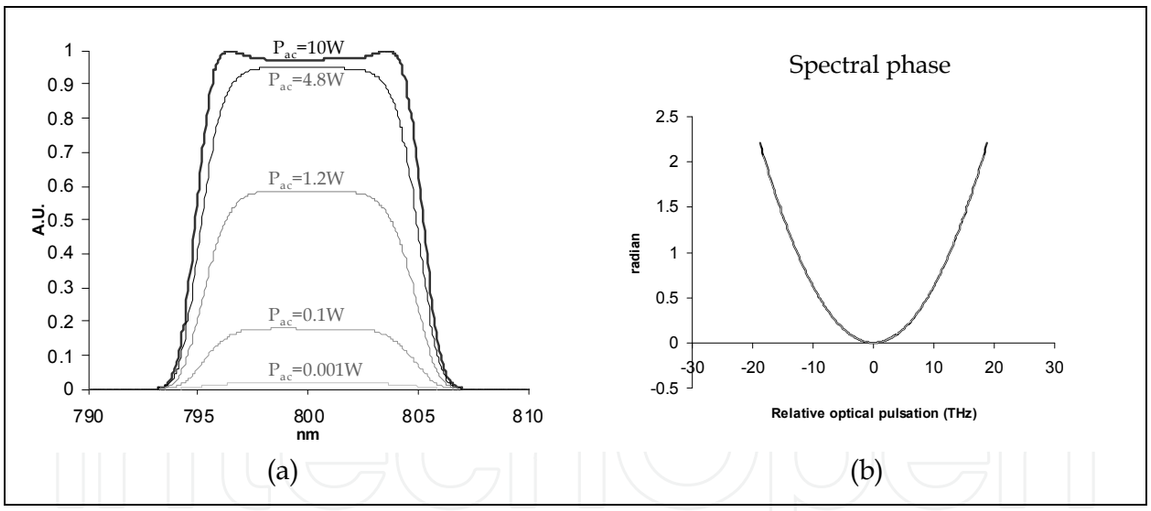

Fig. 7. Simulation of acousto-optic diffraction for (a) spectral amplitude, (b) spectral phase.

The first order can then be used to precompensate the saturation within few percents but exact pulse shaping requires to monitor and loop on the spectral amplitude. The spectral phase is automatically conserved through the Bragg phase matching condition.

4.2.2.2 Acoustic beam limitation

This coupled-wave analysis considers plane waves. Due to the size of the beam relatively to the wavelength, the acoustic wave cannot be considered as a single plane wave. The acoustic beam finite dimension D_a results in the limitation in spatial aperture of each wave that allows to represent the acoustic field in the components of angular spectrum as:

$$\begin{aligned} e_{ac}\left(t,X_{ac},Z_{ac},\xi,\omega_{ac}\right) &= A\left(\xi,\omega_{ac}\right)\exp\left[i\left(\omega_{ac,0}t+K_{\varphi z_{ac}}Z_{ac}+K_{\varphi x_{ac}}X_{ac}\right)\right] \\ &= \frac{A_0 L D_a}{2}\sin c\left(\frac{\left(\omega_{ac}-\omega_0\right)L}{2V_0}\right)\sin c\left(\frac{\omega_{ac}\sin\left(\xi\right)D_a}{2V\left(\xi\right)}\right) \\ &\times\exp\left[i\left(\omega_0 t+\frac{\omega_{ac}}{\mathrm{V}\left(\xi\right)}\cos\left(\xi\right)Z_{ac}+\frac{\omega_{ac}}{\mathrm{V}\left(\xi\right)}\sin\left(\xi\right)X_{ac}\right)\right]. \end{aligned} \tag{77}$$

where X_{ac} and Z_{ac} are the coordinate along the acoustic central wavevector (cf. fig.10), ξ is the relative angle between the wavevector and the Z_{ac} direction, ω_{ac} the acoustic pulsation ($\omega_{ac}=2\pi f_{ac}$), $A(\xi,\omega_{ac})$ the amplitude of the acoustic plane wave of direction ξ and frequency ω_{ac}, $\omega_{ac,0}$ the central acoustic pulsation ($\omega_{ac,0}=2\pi f_{ac,0}$).
Due to the strong anisotropy of the crystal (Zaitsev (2003)), the phase matching condition or Bragg synchronism condition can be rewritten as:

$$\delta k\left(\xi\right)=2\pi\left[\frac{\Delta n}{\lambda}\cos^2\theta_0-\frac{\omega_{ac}\left(\xi\right)}{2\pi V\left(\xi\right)}\cos\left(\theta_0-\theta_a+\xi\right)\right]=0\Leftrightarrow\frac{\lambda\omega_{ac}\left(\xi\right)}{2\pi V\left(\xi\right)\Delta n}=\frac{\cos^2\left(\theta_0\right)}{\cos\left(\theta_0-\theta_a+\xi\right)} \tag{78}$$

The acoustic matched frequency can be expressed from the other parameters as:

$$\omega_{ac}\left(\xi\right)=\frac{\omega_{ac}\left(0\right)V\left(\xi\right)\cos\left(\theta_0-\theta_a\right)}{V\left(0\right)\cos\left(\theta_0-\theta_a+\xi\right)}. \tag{79}$$

The expression for the diffracted light field can be written as a superposition of plane waves:

$$E_d(t,X_{ac},Z_{ac})\propto\int E_{in}(t,X_{ac},Z_{ac})e_{ac}\left(t,X_{ac},Z_{ac},\xi,\omega_{ac}\left(\xi\right)\right)d\xi. \tag{80}$$

The intensity of the diffrated field can be expressed as the superposition of the plane wave contribution with propagation angle ξ:

$$I_d\left(\omega_0\right)\propto\int_{-\pi/2}^{\pi/2}\sin c^2\left[\frac{L}{2V_0}\left(\omega_{ac}\left(\xi\right)-\omega_0\right)\right]\sin c^2\left[\omega_{ac}\left(\xi\right)\sin\xi\frac{D_a}{2V_0}\right]d\xi\,. \tag{81}$$

The acoustic wave velocity can be developped under a small deviation of the angle ξ as:

$$\begin{aligned} &V\left(\xi\right)=V_0\left(1+a\xi+b\xi^2\right), \\ &\text{where } a=-\cot\left(\theta_0-\theta_a\right), \\ &b=\frac{\left({V_{001}}^2-{V_{110}}^2\right)}{2{V_0}^2}\left(\cos 2\theta_a-\frac{\left({V_{001}}^2-{V_{110}}^2\right)}{4{V_0}^2}\sin 2\theta_a\right), \end{aligned} \tag{82}$$

a characterizes the acoustic "walk-off" angle and b is the acoustic field spread.
The acoustic pulsation changes on the angle according to the parabolic law:

$$\omega_{ac}\left(\xi\right)=\omega_{ac,0}\left[1+\left(b+1/2\right)\xi^2\right]. \tag{83}$$

The diffracted field intensity has the form

$$I_d(\omega_0) \propto \int_{-\pi/2}^{\pi/2} \sin c^2\left[\frac{L\omega_{ac,0}}{2V_0}\left[1+\left(b+1/2\right)\xi^2\right]-\omega_0\right]\sin c^2\left[\frac{\omega_{ac,0}\xi}{V_0}\frac{D_a}{2}\right]d\xi\,. \tag{84}$$

As expected from the first order theory, any divergence of the beams decreases the resolution of the device. While optical beam direction modifies mostly linearly the peak diffraction position in frequency, the acoustic direction has a quadratic dependance in the AOPDF configuration which modifies the symetry of the diffracted field intensity profile versus the frequency (or wavelength) as shown on figure 8.

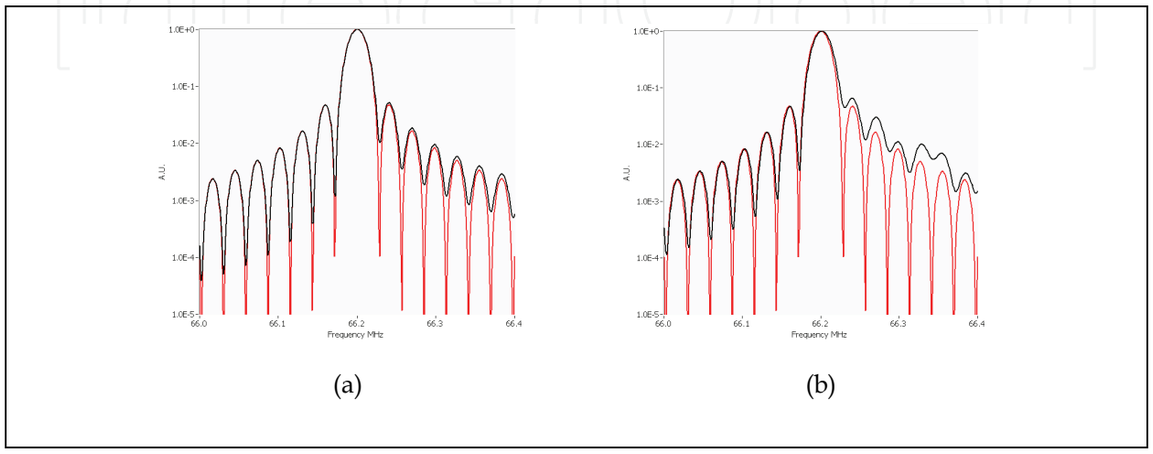

Fig. 8. Simulation of acousto-optic diffraction for (a) D_a=8mm, L=25mm, (b) D_a=2mm, L=25mm, the black and red curves are respectively with and without acoustic beam limitation.

Considering a gaussian optical beam of 2mm at 800nm, its rayleigh length is z_R=15m and its divergence about $\delta\theta \approx 250\mu$rad. Without initial divergence, the resolution of the device is not affected by such a divergence.
This effect can be combined with the multi-frequencies through the momentum mismatch δk of optical and acoustic wave vectors:

$$\delta k(\xi) = k_{0z} - k_{1z} + K_z\left(\omega_{ac}(\xi)\right) = 2\pi\left[\frac{\Delta n}{\lambda}\cos^2\theta_0 - \frac{\omega_{ac}(\xi)}{2\pi V(\xi)}\cos\left(\theta_0 - \theta_a + \xi\right)\right] \tag{85}$$

and summation over the acoustic spectral and spatial frequencies.
These effects can be neglected in standard configuration.

4.2.2.3 Walk-off contribution

The main physical effect not already considered is the walk-off of the diffracted beam and of the acoustic beam. These walk-offs are due to the anisotropy of the crystal. The figure 13 illustrates the two walk-offs and their consequences on the output diffracted beam.
These effects combine each other also with the diffracted beam direction dispersion and finally result in a diffracted beam whose angular chirp is compensated by an adequate output face orientation but the spatial chirp illustrated on fig.9.a still remains. The effect is only a variation of the position of the different frequencies spatially. The maximum value corresponds to the walk-off over the complete crystal length and is given in table 1 for the

different crystals. By opposition to the 4f-line, this effect is not a coupling between optical frequencies and beam direction but rather a coupling between optical frequencies and beam position. The consequence of this coupling on a focal spot is very small.

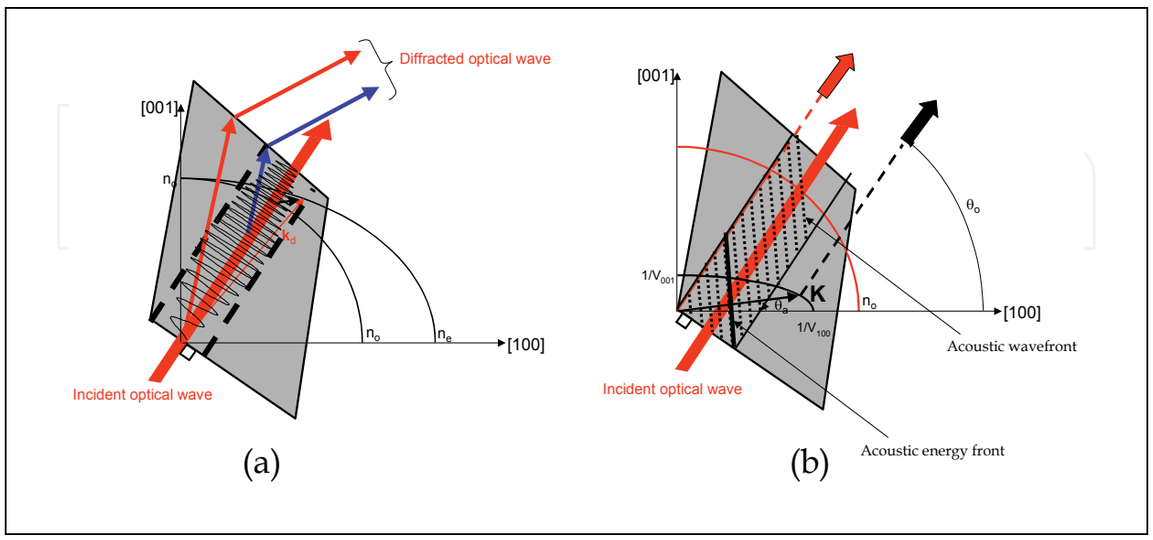

Fig. 9. Illustration of optical walk-off (a), acoustic walk-off (b).

The simulation of the device considering the walk-offs requires the following steps:

1. An input beam E(x,t,0) is propagated from its origin to the diaphragm aperture of the AOPDF by Fresnel propagation.
2. An iris aperture of diameter D_{iris} spatially filters the beam:
   $E(x,t,z) \rightarrow \mathrm{Rect}(x/D_{iris})E(x,t,z)$
3. The spatio-temporal response fonction of the AOPDF H(x,ω) is applied to the pulse
4. The beam is propagated a distance L to the lens
5. A thin lens of focal length f_L is applied
6. The beam is propagated to the focal plane.

The spatio-temporal caracteristics of the pulse shaping are directly include in the filter response function H(x,ω). This function is estimated from the desired ideal filter function $H(\omega)=A(\omega)\exp(i\phi(\omega))$ by applying the following algorithm:

1. Estimation of the dispersion of the crystal
2. Adding the compensation of the spectral phase introduced by the crystal to the output phase
3. Determination of the acoustic wave in the crystal
4. Determination of the crystal length L(x) integrating the prismatic output face
5. Estimation of the acoustic temporal window corresponding to L(x)
6. Introduction of the acoustic walk-off
7. Estimation of the acoustic filter function $H_{ac}(x,\omega)$
8. For each x, calculus of the acoustic delay $\tau(\omega_{ac})$ and determination of its longitudinal position in the crystal : $Z(x,\omega_{ac})$
9. Estimation of the walk-off for each pulsation: $W(\omega_{ac})$
10. For each ω_{ac}, an effective walk-off displacement X is estimated : $X(\omega_{ac})$
11. The filter optical function is calculated from $H_{ac}(x,\omega)$ including saturation of the diffraction and its correction: H(x,ω)

12. The ouput pulse is estimated by multiplying the input pulse $E(x,\omega)$ by the filter function $H(x,\omega)$ and applying the walk-off as $E_{out}(x,\omega)=E_{out}(x-X(\omega),\omega)$.

This model strongest hypothesis is the localization of the diffraction at a specific position $Z(x,\omega_{ac})$. As long as the bandwidth is large enough, this hypothesis is valid.
In the extreme case, a monochromatic acoustic wave fills completely the crystal. There are no specific position but in the same time there are no chromatic displacement at the output because of the monochromaticity!
Figure 10 shows simulation of a chirp, a delay and two pulses for the temporal intensity.

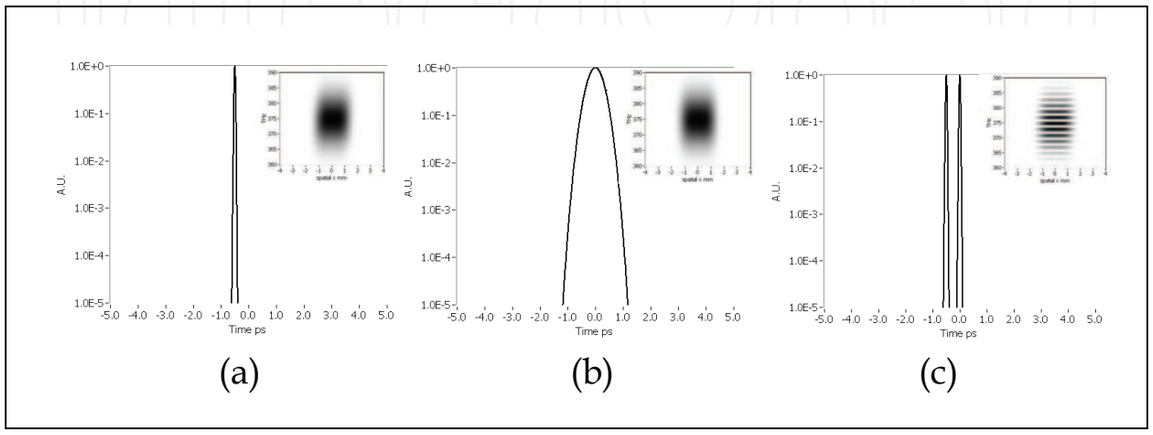

Fig. 10. AOPDF simulation including walk-off, temporal intensity in logarithmic scale and spatio-temporal vizualisation (inset) for (a) a 500fs delay, (b) a chirp 10000fs², (c) two pulses delayed by 500fs.

4.2.3 Conclusions on AOPDFs

The AOPDF devices are bulk and all the characteristics depend upon the parameters of the crystal. Different orientations and crystal lengths give either higher diffraction efficiency or higher resolution from 3ps, 0.6nm to 14ps,0.15nm at 800nm. The principal limitations are :

- the limited length of the crystal limiting the temporal window,
- the propagation of the acoustic wave (about 30µs for the crystal length),
- the efficiency of diffraction.

The crystal cuts optimization is a trade-off between the temporal window maximization and the efficiency of diffraction. The efficiency is determined by the acoustic power for each wavelength. This power depends upon the acoustic pulse shape and the maximal RF power acceptable by the transducer for the acoustic generation. This power is in the range of 10W. With an optimal chirp acoustic pulse high efficiency of diffraction can be achieved over large bandwidth. But if the acoustic pulse is compressed, then all the wavelength "share" the 10W peak power. This effect can decrease the efficiency of diffraction by an important factor. For example compensation of third order spectral phase influences the efficiency of diffraction.
The propagation of the acoustic wave through the crystal at about 720m/s implies to synchronize the acoustic wave generation with the optical pulse. The jitter on the synchronization has a direct incidence on the absolute phase of the diffracted pulse. The delay in acoustic generation can be directly linked to the optical delay by the acoustic and optical temporal windows lengths. This effect will be review on the CEP control off the

pulse. As the crystal length equivalent acoustic duration is about 30μs, a single acoustic wave can be synchronized perfectly with a single optical pulse only for laser repetition rate below 30kHz. For higher repetition rate, laser pulses will be diffracted by a same acoustic pulse at different position in the crystal leading to distortions.
As seen on the Fig.10, the walk-off in the crystal modifies spatially the output beam. The main effect is to spread the different wavelength at different positions. Depending upon the crystal caracteristics, the maximal displacement is in the range of 0.5mm or 1.5mm. This effect can be completely nullify by a double pass configuration as shown in the experimental implementations.

5. Pulse shaping examples

In this section, we compare the results obtain with the two technologies simulated with the models described in the previous part on identical pulse shaping examples. The ultrashort pulse considered is 20fs gaussian shape with a 2.3mm spatial gaussian shape.
This pulse will be pulse shaped by the four devices (table 3) to obtain first the best compressed pulse at the focal point of a perfect lens with an initial dispersion of 2000fs^2 and 50000fs^3 at 800nm, secondly a square pulse with a time/bandwidth product of 100, thirdly double pulses.
The table 3 sums up the parameters and caracteristics of the different pulse shapers used in this part at 800nm.

Parameters	4f-SLM 128 pixel pitch=100μm gap=3μm f=200mm $\theta_l=\theta_d=20$deg p=600lines/mm	4f-SLM 640 pixel pitch=100μm gap=3μm f=500mm $\theta_l=\theta_d=20$deg p=1200lines/mm	AOPDF WB25	AOPDF HR45
Spectral resolution $\delta\lambda$ nm	0.8	0.16	0.6	0.15
Bandwidth $\Delta\lambda$ nm	100	100	>200	>200
Temporal window @ 3dB (10%)	2.5ps	12 ps	3ps	15ps
Spatio-temporal slope or maximal walk-off	0.783mm/ps	0.293mm/ps	0.2mm/ps	0.1mm/ps
Number of points on 100nm	128	640	167	667

Table 3. Pulse shapers parameters.

5.1 Compressed pulses and focal spots

In this part, we simulate the compression obtained for (1) a pulse but stretched by 2000fs^2 and 50000fs^3 spectral phase with a gaussian shape of 50nm full-width at half-maximum, 2.3mm diameter. The compressed pulse for each pulse shaper will be caracterized on for its ps contrast, and the comparison between ideal compressed pulse energy distribution around the focus and the simulated one.
The ps contrast is shown directly by the intensity profile on a logarithmic scale.
The energy distribution is represented by plotting the energy distribution in the focal spot area and its difference with the ideally compressed pulse.
The initial pulse is stretched in time over about 100fs by the chirp and with a trailing edge due to the third order spectral phase on one ps at 10^{-6}. The compression of this pulse by the

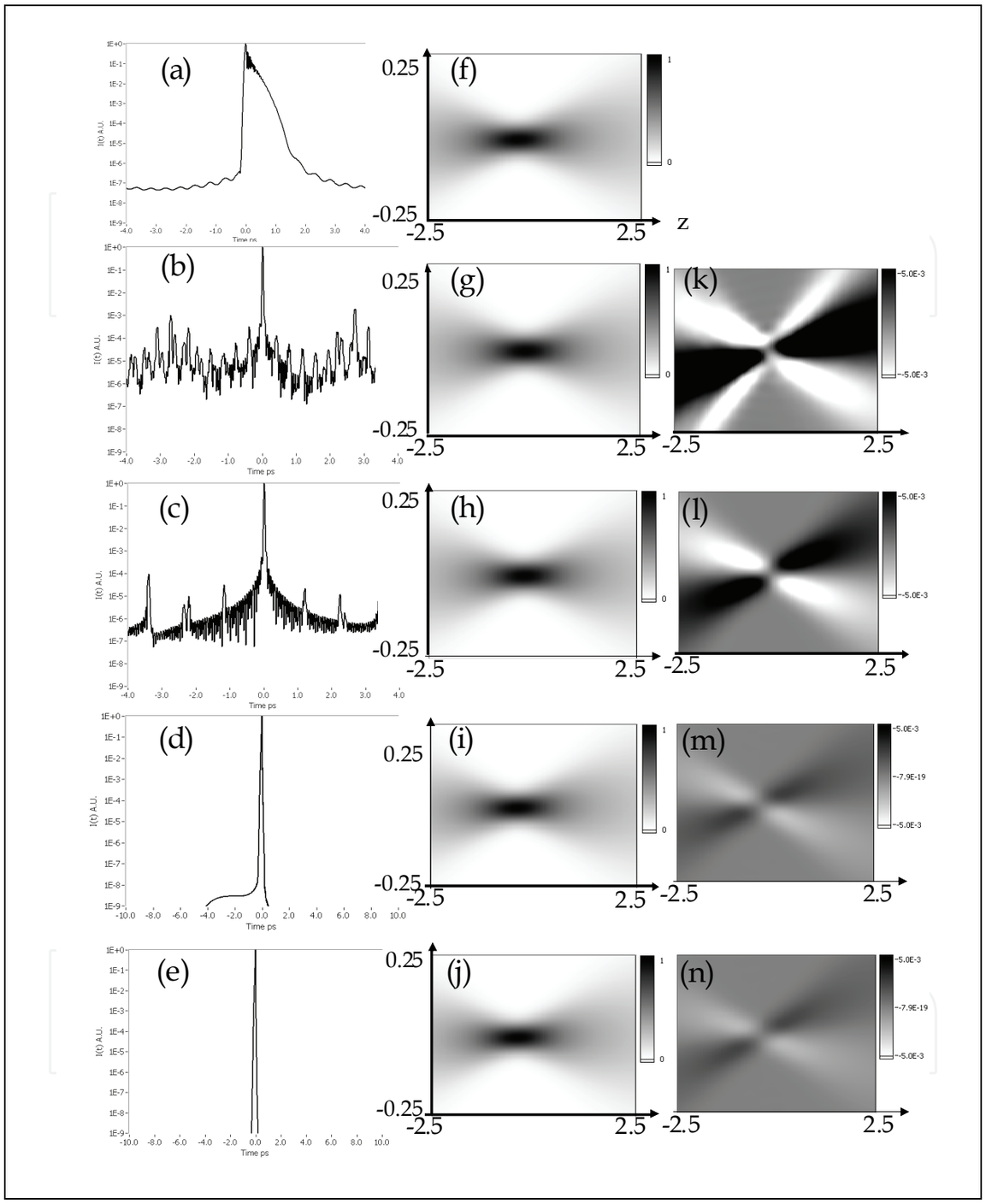

Fig. 11. Compression of 50nm gaussian shape pulse with $\phi^{(2)}$=2000fs^2 and $\phi^{(3)}$=50000fs^3. The first column shows the temporal intensities in logarithmic scale of (a) initial stretched pulse, (b) SLM128 compression, (c) SLM640 compression, (d) AOPDF WB25 compression, (e) AOPDF HR45. The second and third columns contain respectively peak power and energy distribution maps for respectively (f) initial stretched pulse, (g,k) SLM128, (h,l) SLM640, (i,m) AOPDF WB25, (j,n) AOPDF HR45.

pulse shaper points out specificities on the contrast. Due to pixelization, phase wraps and smoothing, the SLM128 and SLM640 4f-pulse shapers create pulse replicas at a level 10^{-3} and 10^{-4} respictevely. These pulses mainly due to gaps, pixelization and phase wraps are on top-off a background at 10^{-6} due to pixel smoothing. On the focal spots the deviation of the energy distribution is about 1% for these two devices. The AOPDFs recompression leads to a pulse without any temporal alteration for the High Resolution 45 device and a small pedestal at 10^{-8} for the Wide Band 25. This pedestal is due to a cut of the acoustic wave which is slightly longer than the crystal itself. On the focal spot the effect of the walk-off is more than 10 times smaller than for 4-f pulse shaper.
High contrast compression of pulses clearly requires no pixelization, gaps, phase wraps or smoothing and thus is better achieved by AOPDFs.

5.2 Square pulse with Time/Bandwidth product >100

Temporal square pulses are of interest both for Free Electron Laser electron bunch seeding and for optical parametric amplification pumping. The temporal intensity required has fast rise time (<500fs) and a flat top pulse without ripples. The very first idea to obtain such a pulse is to apply a flat temporal phase and Fourier transform the square root of this temporal intensity profile. This leads to a spectral amplitude with a sinus cardinal shape. This shape has a large pedestal bandwidth and a relatively narrow central peak. Considering that the initial pulse to shape has a gaussian shape with 50nm fwhm, obtaining a 2.3ps square pulse with a sinus cardinal spectral shape will loose most of the energy and required a very precise shaping on the edge of the spectrum.

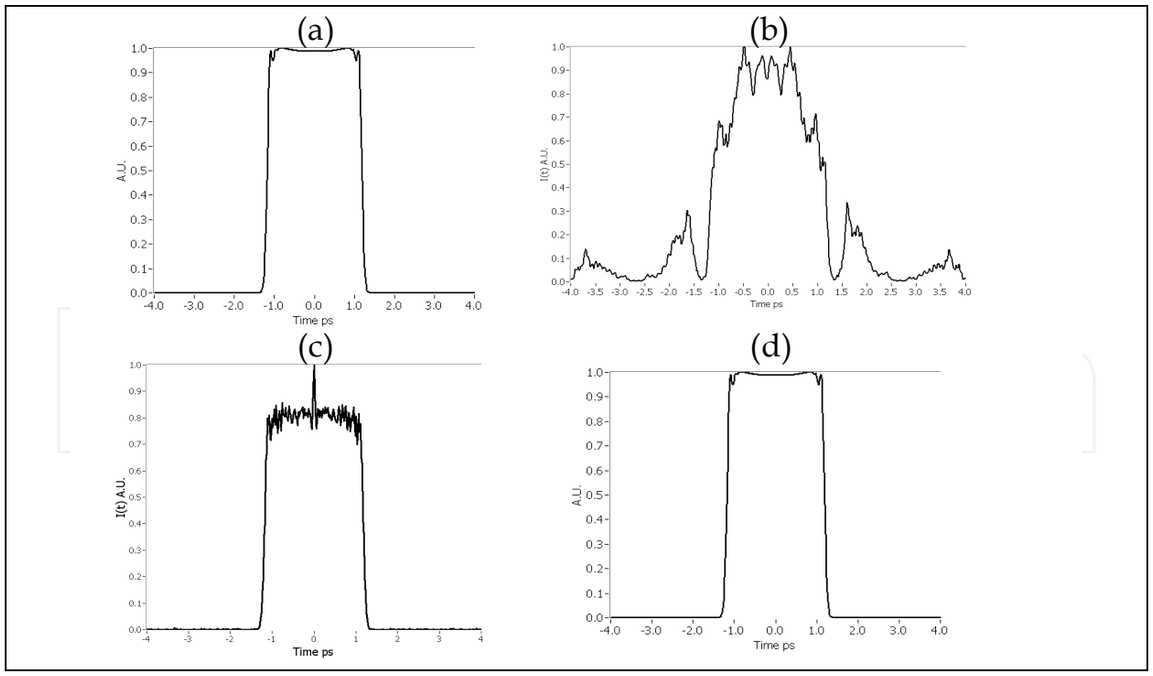

Fig. 12. Creation of a square temporal intensity pulse from a 50nm gaussian shape Fourier transform pulse by applying an amplitude filter super gaussian of order 6 with a fwhm of 52nm and a spectral phase with $\phi^{(2)}= 20\ 10^3$ fs2,$\phi^{(4)}=-5.2\ 10^6$ fs^4, $\phi^{(6)}= 600\ 10^6$ fs^6, with (a) ideal pulse shaper, (b) SLM128, (c) SLM640, (d) AOPDF WB25 or AOPDF HR45.

If no temporal phase shape is required, the optimal shape is a mix of amplitude and phase shaping. The fast rise time will be obtain by linear phase on the sides, the flat top by a chirp. The optimal shaping is obtained by applying a super gaussian amplitude filter of order 6 and fwhm 52nm on top of the 50nm fwhm gaussian spectrum, and a spectral phase composed by $\phi^{(2)}= 20\ 10^3$ fs2,$\phi^{(4)}=-5.2\ 10^6$ fs^4, $\phi^{(6)}= 600\ 10^6$ fs^6. Such pulse shaping is shown on the fig.16 below for the different pulse shapers and for an initial Fourier transform pulse.

The effects of pixelization and smoothing clearly modify the temporal shape for the 4-f pulse shapers. The effect of the beam size is not taken into account in this simulation. The central peak for the SLM640 pulse shaper can be compensated as proposed by Wefers and Nelson but only by an experimental feedback loop. This kind of feedback loop depends upon the measurement technique and accuracy. For the AOPDF, no default appears as long as the acoustic wave fits in the crystal.

5.3 Double pulses

To evaluate the quality of the pulse shaping for compressed pulse at the focal spot, three parameters are considered: the temporal intensity integrated over the focal volume considered; the spatial overlap integrals, within the focal volume, between frequencies; the relative strength of multiphoton transition probabilities, integrated across the focal volume. The last parameters have been introduced by Sussman [2008] to be relevant criteria in multiphoton experiments. The normalized overlap integrals measure the spatial variation of different colors through the focus:

$$O_{\lambda_1\lambda_2} = \frac{\int I_{\lambda_1} I_{\lambda_2} dxdz}{\sqrt{\left(\int {I_{\lambda_1}}^2 dxdz \int {I_{\lambda_2}}^2 dxdz\right)}}, \tag{86}$$

where $I_{\lambda 1}(x,z)$ represents the field intensity for a particular wavelength. The values of the overlap integrals $O_{\lambda 1\lambda 2}$ may vary considerably. A value of 1 indicates that two colors have a complete overlap throughout the focal volume. Variations below 1 are significant for any multiphoton experiments.

The probability for a vertical n-photon transition having no intermediate resonances is given by the nth-order power spectrum:

$$P_n \propto \left|\int \left(E(t,x,z)\right)^n e^{-i\omega t} dt\right|^2. \tag{87}$$

Without space-time coupling, this transition probability is proportionnal to the peak intensity I at a point: $P_n \propto I^n$. Therefore, the ratio between the nth-order and the mth-order multiphoton transitions $P_n/P_m^{n/m}$ should be constant if only the peak intensity – and not the spectral content- at a spatial point is altered. In order to quantify this effect, this ratio is integrated over the focal volume, normalized and compare with the non space-time coupled one as

$$r_{mn} = \frac{\int \left|\left(P_n / P_m^{\,n/m}\right) - 1\right| dxdz}{\int dxdz}. \tag{88}$$

In the absence of space-time coupling, these values would be zero. However, since the spectral content at each point is modified, the ratios are not constant and their deviation

from 1 can be considerable. The global value is integrated over the volume of interest, for example the focal volume.

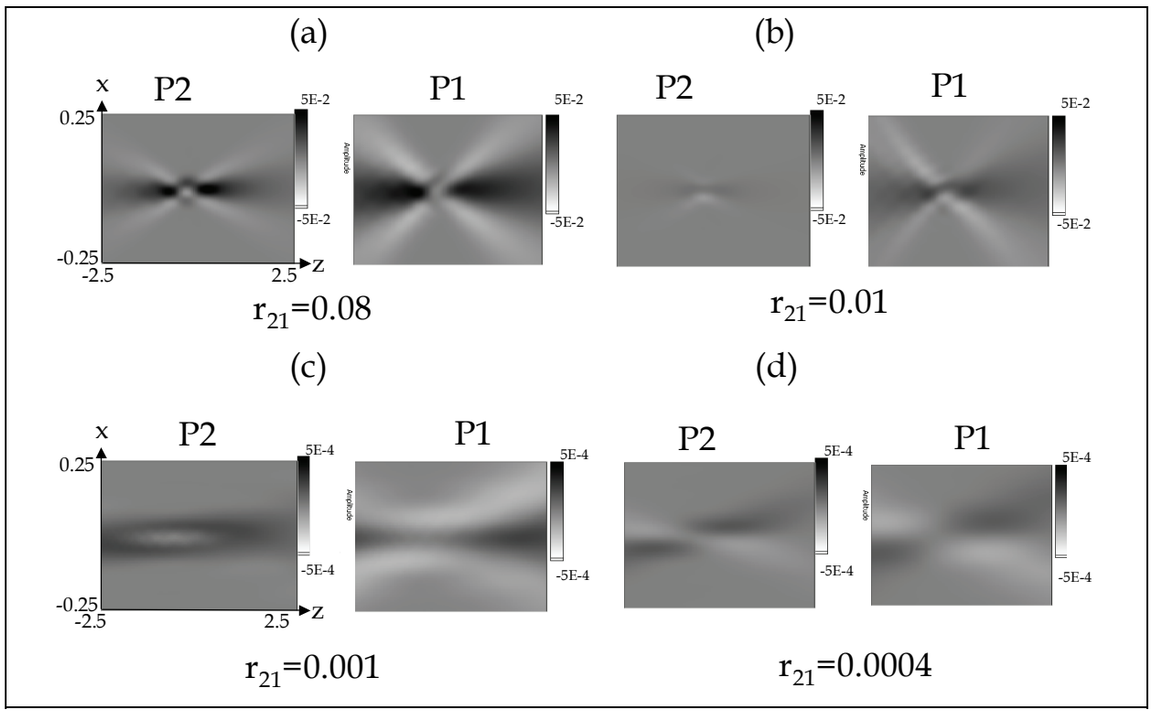

Fig. 13. Comparison of two pulses delayed by +250fs and –250fs and maps of the differences of energy P1 and power P2 at the focal plane of a 100m focal length lens for (a) SLM128, (b) SLM640, (c) AOPDF WB25 and (d) AOPDF HR45.

The influence of the spatio-temporal coupling is caracterized both by the r_{21} ratio and the energy and power difference maps. As pointed out by the spatio-temporal parameter, the SLM128 has the highest coupling, and the AOPDF HR45 the lowest. These effects can be very important when the pulse shaper is used to optimize a non linear effect at the focus on a non strictely homogeneous media. Indeed, modification of the spatial profile instead of the temporal one can be the predominant effect in the optimization.

5.4 Conclusions

Depending upon the relevant parameters of a pulse shaping experiment, the pulse shaper has to be adapted. An adequate simulation of the pulse shaper should estimate the minimum requirements. Also experimental implementation and alignement tolerances that are beyond the scope of this chapter should be taken into account. Feedback loop can be used to optimize the temporal shape. But some inherent defaults of the pulse shaping technology can also compromise the experimental results and cannot be compensated by any feedback loop. Moreover the accuracy and dynamic of the measurement that should be used for the loop is already an experimental challenging part.

6. Experimental implementations

This part gives examples of experimental implementations of pulse shaping with their advantages and limitations. As pulse shapers can be applied to a wide range of applications,

experimental implementations are reviewed in the scope of the laser source from oscillators to multi-TeraWatt laser systems. Example of feedback loop with measurement devices will also be given.

6.1 Oscillators

Applications of pulse shaping with oscillators are direct pulse shaping of the output train of pulses. Among them are for examples, multiphoton microscope imaging, white light optimization for spectroscopy. The pulse shaper is used directly before the experiment.
For 4-f pulse shaper there are no modification of the pulse shaping response function due to the high repetition rate of the laser. The mask can be considered as fix. An imaging relay optics should be used to avoid magnification of the space-time coupling effects [Tanabe (2005)]. Many different kind of experiments have benefit from optimization by feedback loop such as multiphoton microscopy or coherent control (fig.14). This feedback can be either used to optimize the pulse shape [Coello 2008], or to directly optimize an experimental result by blind algorithms [Assion 1998, Brixner 2000]. Refreshing rate of standard LC SLM is about few tens of millisecond. Higher modulation refreshing rate can be obtain by using two lines LC SLM and switching from one line to the other.
For AOPDF, the acoustic wave is moving at 720m/s in the crystal. Therefore, the acoustic pulse is moving in the crystal from pulse to pulse. Synchronization of the measurement system with the acoustic wave is then needed to eliminate the measurement with a partial acoustic wave in the crystal. In standard 25mm crystals, the complete acoustic time window is about 30µs. Thus depending upon the duration of the acoustic wave (Δt_a) used for the shaping, this acoustic wave is totally include in the crystal during 30µs-Δt_a. The measurement has to be gated on during this time and off in between to consecutive acoustic pulse (Δt_a) (fig.14). This drawback of AOPDF can be overcomed by its higher refreshing rate (up to 30kHz) that can be used for differential measurements between two pulses shapes [Ogilivie 2006] eventually with heterodyne detection.

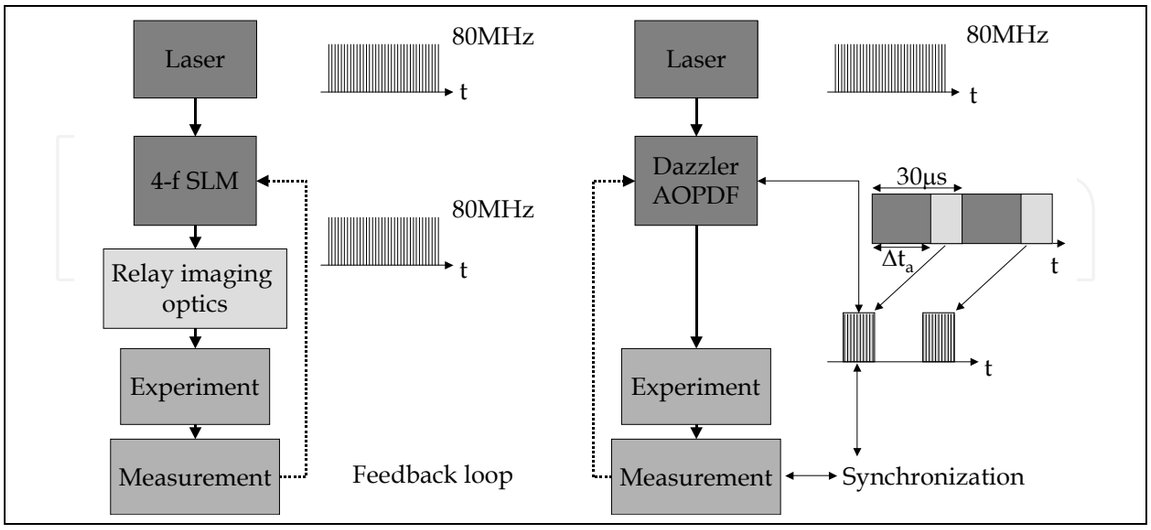

Fig. 14. Implementation of 4-f pulse shaper and AOPDF at the output of an oscillator.

New implementations of these two techniques for multiphoton or CARS microscopy, coherent control are currently published demonstrating higher efficiency or sensitivity.

6.2 Amplified systems

In amplified system, depending upon the damage threshold energy and non linearities in the pulse shaper, the device is inserted in the laser chain or at the output.

The irradiance limit ($W.m^{-2}$) of pulse shaper is different for AOPDF and for 4f-pulse shaper. For AOPDF, this limit is defined upon the non-linearities in the massive TeO2 crystal. To avoid any significative distorsion, this limit is defined as an upper value of cumulative effect of self-phase modulation (B-integral):

$$B = \max\left(\varphi_{nonlinear}\right) = \max\left(\int \frac{2\pi}{\lambda} n_2 I(t,l)\, dl\right), \tag{89}$$

where n_2 is the nonlinear index ($n_2 \approx 23 \times 10^{-13}$esu $\approx 67 \times 10^{-16}$ cm^2/W for TeO_2), λ is the optical wavelength, I(t,l) the irradiance or intensity ($W.m^{-2}$). Depending upon the tolerances on spatial and temporal distorsions due to this slef-phase modulation, the B-integral limit is set to 0.1, 1 or π [Perry (1994)]. Considering a medium value of 1, the input irradiance can be up to $200\mu J/cm^2$ for 30fs pulses [Monmayrant (2005)]. This value includes the dispersion of the pulse by the crystal itself. A $200\mu J/cm^2$ pulse of 25fs and a $220\mu J/cm^2$ pulse of 35fs at 800nm lead to the same B-intergal of 1. Thus depending upon the pulse duration and size, pulses up to mJ level can be used with AOPDF before compression.

For 4f-pulse shaper, the gratings can have high damage threshold and the limitation is about $1GW/cm^2$. This implies that a 4f-pulse shaper can be used at the output of an amplified system at the milliJoule level.

The figure 15 details the different position where the pulse shaper can be inserted. The stretcher and compressor are linear elements and do not affect the pulse shaping. The amplifier can be either a CPA amplifier or an optical parametric amplifier. Amplifiers are in general non linear because of saturation, red shift, four wave mixing [Liu (1995)].

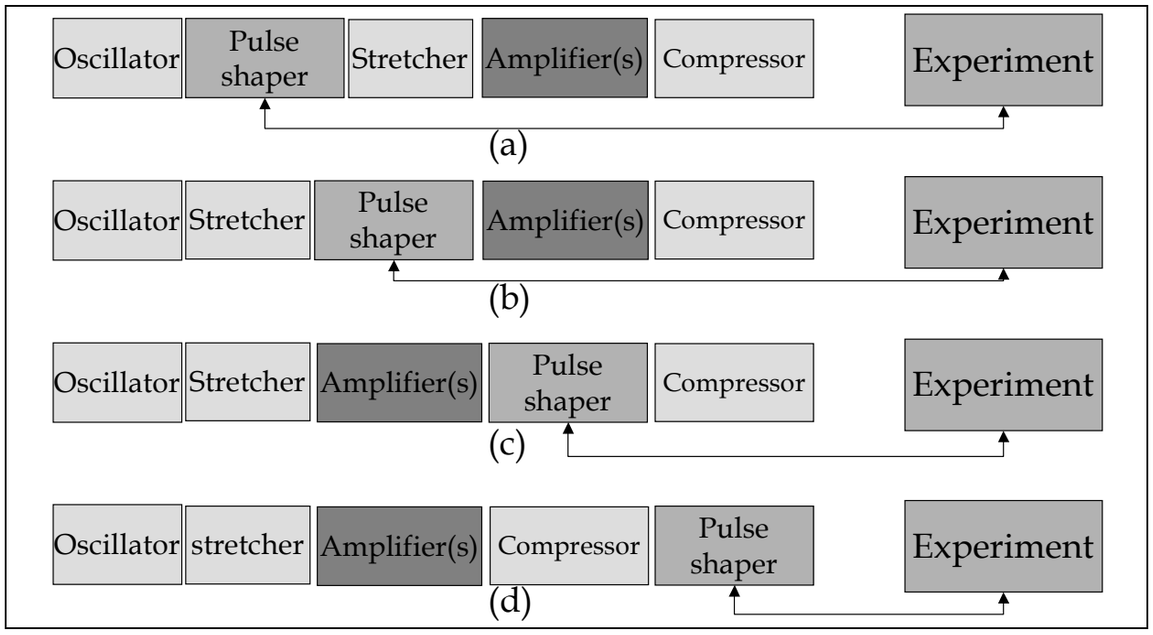

Fig. 15. Implementations of a pulse shaper amplified systems: (a), (b) indirect pulse shaping, (c), (d) direct pulse shaping.

Depending upon the position of the pulse shaper, before or after the "non linear" element, the amplifier(s), the shaping will be linear or not. The linear case is "named direct pulse shaping" because the shaping will be transmitted from the pulse shaper to the experiment directly. In the non linear case, or "indirect pulse shaping", the shaping introduced is altered by the non linear element. Indeed, as the amplification distords the spectral amplitude, when the pulse shaper is inserted before the amplifier, the shaping is modified by the amplifier. Indirect pulse shaping restricts the possibilities of pulse shaping as mentionned in the Special Topics hereafter. As an example, a double pulse injected in the amplifier will result in multiple pulses at the output [Liu (1995), Boyle (2001)]. Limitations are due the amplifier caracteristics. In CPA systems, the phase shaping can be considered as a small perturbation of the Chirped introduced and is generally conserved linearly through the amplification. Main limitation comes from spectral amplitude distorsions. Part of the distortions can be pre-compensated by a feedback loop but not all of them.

6.3 Feedback loops

As mentionned previously, there is a strong interest of feeding back the pulse shaper with measurements of the shaped pulses. This loop can overcome some defaults of the pulse shaper or optimize experimental results such as compression via non linear generation optimization or specific excitation in coeherent control.

To illustrate such a loop, optimization of the pulse duration by flattening the spectral phase will be described for the two techniques.

Many publications describes feedback loop for optimization with 4f-pulse shaper after amplification but very few with the shaper before the amplifier. When the pulse shaper is directly before the amplifier, the feedback loop is used to overcome inaccuracy of the pulse shaper. Few publications present loops with advanced measurement devices as Frequency Resolved Optical Gating (FROG) [Kane (1993)] or Spectral Phase Interferometry for Direct Electric-field Reconstruction (SPIDER) [Iaconis (1998)] with 4f-pulse shaper. Direct shaping optimization with a SPIDER (pulse shaper just in front of the SPIDER) on a ultrashort pulse (3.8fs) requires 5 iterations [Schenkel (2003)].

For AOPDF, optimization in indirect pulse shaping configuration with a SPIDER is regularly used in CPA laser system with a single correction step.

This feedback loop can be sketched as:

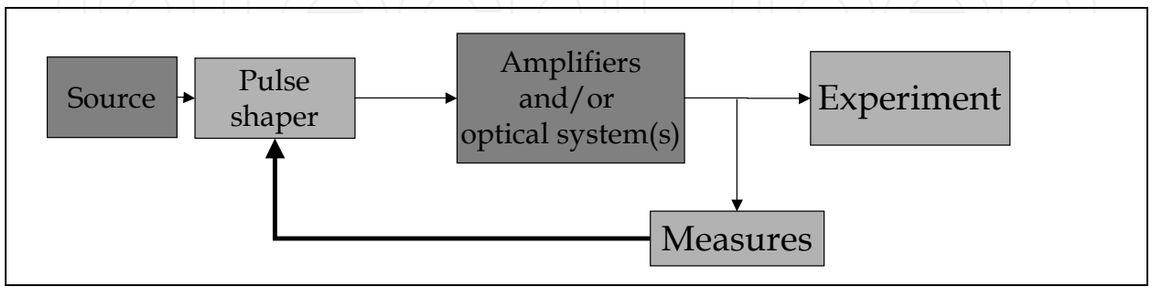

Fig. 16. Implementations of a pulse shaper feedback loop for pulse compression optimization.

The feeding parameters are the spectral amplitude and phase, but they can be obtained through different type of mesurements. With SPIDER, care should be taken on the spectral

phase on the sides of the spectrum where the measurement is inaccurate. Polynomial prolongation from valid area of measurement shouold be used to avoid significant cut due to the pulse shaping [Oksenhendler (2003)]. With FROG, the feedback is more efficient if done by direct reference to FROG traces [Ohno (2002)].
In conclusion, implementing a feedback loop with a pulse shaper can overcome indirect shaping or inaccuracy of the pulse shaper. Special attention should be taken onto convergence and limitation problem. As an example if the compression of the pulse requires a shaping that is out of the scope of the pulse shaper used, the optimal solution will not be the compressed pulse (best optimum) but a second and local optimum that can be achevied by the pulse shaper. User should check that the solution seeked is in the scope of the loop.

7. Special topics

As described previously, a precise determination of the key parameters of the experiment should be done to select and adapt the proper pulse shaping technology. This part deals with some examples that are experimentally important and point out the relevant parameters to consider and the technologies that can be applied.

7.1 Carrier Envelope Phase control

In attosecond pulse generation, the Carrier Envelope Phase has to be stable to get a stable generation. The time dependence of the electric field associated with an optical pulse can be described as a fast sinusoidal oscillation, called the carrier, multiplied by a more slowly varying envelope function. When the pulse propagates through a medium, the relative position between the carrier wave and envelope will in general change due to chromatic dispersion causing a difference between phase velocity and group veocity, and possibly also due to optical nonlinearities. The carrier envelope offset phase (or absolute phase) of a pulse is defined as the difference between the phase of the carrier wave and the envelope position, the latter being converted to a phase value.
As the pulse shaper has the ability to control directly the realtive absolute phase, it can control the carrier envelope phase.
For a 4-f pulse shaper, this phase is directly introduced by the mask and can be changed at the refreshing time of the mask (about 10ms). Two effects can introduce fluctuations on the carrier envelope phase: beam pointing fluctuations and mechnanical vibration of the optical components of the pulse shaper.
For an AOPDF pulse shaper, the absolute phase value is directly linked to the phase value of the acoustic wave and its relative position in the crystal. The synchronization of the acoustic wave generation with the optical pulse fixes this position. A delay of $\delta\tau$ on this acoustic synchronization will result in an optical delay $\delta\tau_{opt} \approx \delta\tau(3ps/30\mu s)$. This delay introduces a modification of the absolute phase $\delta\phi = 2\pi(\delta\tau_{opt}.f_{opt})$. So for a phase modification lower than $\pi/20$, the jitter on the acoustic wave generation has to be lower than 500ps. This low jitter operation requires a synchronization of the RF clock with the oscillator laser repetition rate. With this synchronization, the AOPDF can control the phase with an accuracy determined by the residual jitter, at refreshing time down to 30kHz. As for 4-f pulse shaper, the beam pointing will affect the carrier envelope phase stability. But mechanical vibration as it is a bulk crystal are less important.

7.2 Indirect pulse shaping

In some experiments, pulse shapers cannot be used directly on the pulse to shape. For example on high peak power TeraWatt laser system, the pulse shaper can't stand the output energy of the laser. In these cases, the pulse shaper is used before non linear systems as amplifiers or non-linear elements. The shaping of the wanted pulse is then obtained through an indirect process. This indirect pulse shaping modifies the possibilities of shaping. For example, with a Ti:Saphire CPA amplifier, the spectral amplitude is modified by redshift as shown on the figure 17. The spectral phase introduced by the pulse shaper is only a perturbation compared with the chirp of the stretcher. The amplifier is linear for the spectral phase and non linear for the amplitude. The limitations on the pulse shapes are due to the distorsion in the amplifier. A feedback loop on the amplitude can overcome some of the distorsions.

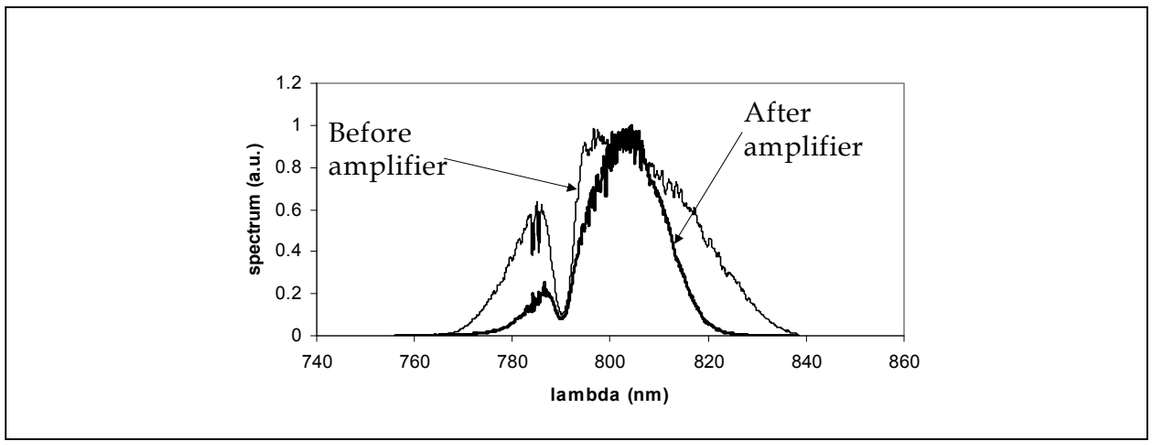

Fig. 17. Indirect pulse shaping.

8. Conclusion

Pulse shaping techniques introduces the concept of linear filter in the field of ultrashort pulses. Optimization of pulse duration, simulation of linear optical set-up (interferometers, pass band filters …) can be achieved, modified or adapted directly by programming different filter function. This capability opens new possibilities such as illustrated by the pulse measurement techniques using an acousto-optic programmable dispersive filter.
An careful analysis of the pulse shaper limitations and defaults such as pulse replica, space-time coupling, should be done, prior to the choice of the pulse shaper technology, to fit the experimental needs.

9. References

Assion A., Baumert T., Bergt M., Brixner T., Kiefer B., Seyfried V., Strehle, Gerber G., "Control of chemical reactions by feedback-optimized phase-shaped femtosecond laser pulses", Science Vol.282, pp. 919-922 (1998)

Boyle M., Thoss A., Zhavaronko N., Korn G., Kaplan D., Oksenhendler T., "Amplitude and phase shaping in a high average power 1kHz CPA-laser", CLEO 2001

Brixner T., Oehrlein A., Strehle M., Gerber G., "Feedback-controlled femtosecond pulse shaping", Appl.Phys.B 70, pp. S119-S124 (2000)

Coello Y., Lozovoy V.V, Gunaratne T.C., Xu B., Borukhovich I., Tseng C.-H. Weinacht T., Dantus M., "Interference without an interferometer: a different approach to measuring, compressing, and shaping ultrashort pulses", JOSA B, Vol.25, pp. A140-A150 (2008)

Danailov M.B., Christov I.P, (1989)."Time-space shaping of light pulses by Fourier optical processing", J.Mod.Opt. Vol 36, 725 (1989).

Dugan M.A., Tull J.X., Warren W.S., (1997). J.Opt.Soc.Am.B Vol.14, 2348 (1997).

Fork R.L., (1981). R.L.Fork, B.I. Greene, C.V.Shank, Appl.Phys.Lett. 38 671 (1981).

Froehly C., Colombeau B., Vampouille M., (1983). *Progressinf Optics*, edited by E.Wolf (north-Holland, Amsterdam, 1983), Vol.20, pp.65-153.

Iaconis C., Walmsley I.A.,"Spectral phase interferometry for direct electric-field reconstruction of ultrashort pulses", Opt.Lett., Vol. 23, pp.792-794 (1998)

Kane D.J., Trebino R., "Single-shot measurement of the intensity and phase of an arbitrary ultrashort pulse by using frequency-resolved optical gating", Opt.Lett., Vol.18, pp. 823-825 (1993)

Khoo I.-C., Wu S.-T., "Optics and nonlinear optics of liquid crystals", World Scientific Publishing, Singapore (1993)

Laude V., "General solution of the coupled-wave equations of acousto-optics", J.Opt.Soc.Am.B, Vol.20, No.12, 2307-2314 (2003)

Liu X., Wagner R., Maksimchuk A., Goodman E., Workman J., Umstadter D., Migus A., "Nonlinear temporal diffraction and frequency shifts resulting from pulse shaping in chirped-pulse amplification systems", Opt.Lett. Vol.20, pp. 1163-1165 (1995)

Martinez O.E., (1986), "Grating and prism compressors in the case of finite beam size", J.Opt.Soc.Am.B vol.3, pp.929-934 (1986)

Monmayrant A., Chatel B., (2003). "Newphase and amplitude high resolution pulse shaper", Rev.Sci.Instrum., Vol.75, No.8, 2668-2671 (2003).

Monmayrant A., "Façonnage et caractérisation d'impulsions ultracourtes. Contrôle cohérent de systèmes simples.", PhD Thesis, Université Paul Sabatier Toulouse III, 2005.

Monmayrant A., Arbouet A., Girard B., Chatel B., Barman A., Whitaker B.J., Kaplan D., "AOPDF-shaped optical parametric amplifier output in the visible", App.Phys.B, 81, pp. 177-180 (2005)

Ogilvie J.P., Débarre D., Solinas X., Martin J.-L., Beaurepaire E., Joffre M. « Use of coherent control for selective two-photon fluorescence microscopy in live organisms", Opt.Expr., Vol.14, pp. 759-766 (2006)

Ohno K., Tanabe T., Kannari F., "Adaptative pulse shaping of phase and amplitude of amplified femtosecond pulse laser by direct reference to frequency-resolved optical gating traces", JOSA B, Vol.19, pp.2781-2790, (2002).

Oksenhendler T., Rousseau P., Herzog R., Gobert O., Perdrix M., Meynadier P., "20Hz Femtosecond laser amplifier optimization using an AOPDF pulse shaper and a SPIDER", CLEO 2003

Oksenhendler T., "Mesures et contrôles temporels dans le domaine des lasers ultrabrefs", PhD thesis, Ecole Polytechnique 2004.

Perry M.D., Ditmire T., Stuart B.C., "Self-phase modulation in chirped-pulse amplification", Opt.Lett, Vol. 19, pp. 2149-2151 (1994)

Schenkel B., Biegert J., Keller U., Vozzi C., Nisoli M., Sansone G., Stagira S., De Silvestri S., Svelto O., "Generation of 3.8fs pulses from adaptative compression of a cascaded hollow fiber supercontinuum", Opt.Lett., Vol.28, pp.1987-1989 (2003)

Strickland D., Mourou G., (1985). "Compression of amplified chirped optical pulses, Opt.Comm. 55, 219-221, (1985)

Sussman B.J., Lausten R., Stolow A., (2008). "Focusing of light following a 4-f pulse shaper: Considerations for quantum control", Phys.Rev.A 77, 043416-1043416-11 (2008).

Tanabe T., Tanabe H., Teramura Y., Kannari F., "Spatiotemporal measurements based on spatial spectral interferometry for ultrashort optical pulses shaped by a Fourier pulse shaper", J.Opt.Soc.Am.B Vol.19,2795-2802 (2002)

Tanabe T., Kannari F., Korte F., Koch J., Chichkov B., "Influence of spatiotemporal coupling induced by an ultrashort laser pulse shaper on a focused beam profile", Appl.Opt. Vol.44, 1092-1098 (2005)

Thurston R.N., Heritage J.P., Weiner A.M., Tomlinson W.J., "Analysis of Picosecond Pulse Shape Synthesis by Spectral Masking in a Grating Compressor", IEEE J.Quantum Electron.22, 682-696 (1986).

Tournois P., "Acousto-optic programmable dispersive filter for adaptative compensation of group delay time dispersion in laser systems", Opt.Comm, Vol.140, 245-249 (1997)

Vaughan J.C., Hornung T., Feurer T., Nelson K.A, (2005). "Diffraction-based femtosecond pulse shaping with a 2D SLM", Opt.Lett. 30, 323-325 (2005).

Vaughan J.C., Feurer T., Stone K.W., Nelson K.A., (2006), "Analysis of replica pulses in femtosecond pulse shaping with pixelated devices", Opt.Exp. Vol.14, No.3,1314-1328 (2006).

Verluise F., Laude V., Cheng Z., Spielmann C., Tournois P., "Amplitude and phase control of ultrashort pulses by use of an acousto-optic programmable dispersive filter: pulse compression and shaping", Opt.Lett. Vol.25, 575-577 (2000)

Wefers M.M., Nelson K.A., (1995). "Analysis of programmable ultrashort waveform generation using liquid-crystal spatial light modulators", J.Opt.Soc.Am.B, Vol.12, No.7, 1343-1362 (1995).

Wefers M.M., Nelson K.A., (1996). "Space-time profiles of shaped ultrafast optical waveforms", IEEE J.Quant.Elec Vol.32, No.1, 161-171 (1996).

Weiner A.M., (2000). "Femtosecond pulse shaping using spatial light modulators", Rev.Sci.Instrum., Vol.71, No.5, 1929-1960 (2000).

Yariv A., Yeh P., "Optical waves in crystals", Wiley, New York, 1984.

Advances in Solid State Lasers Development and Applications

Edited by Mikhail Grishin

ISBN 978-953-7619-80-0
Hard cover, 630 pages
Publisher InTech
Published online 01, February, 2010
Published in print edition February, 2010

Invention of the solid-state laser has initiated the beginning of the laser era. Performance of solid-state lasers improved amazingly during five decades. Nowadays, solid-state lasers remain one of the most rapidly developing branches of laser science and become an increasingly important tool for modern technology. This book represents a selection of chapters exhibiting various investigation directions in the field of solid-state lasers and the cutting edge of related applications. The materials are contributed by leading researchers and each chapter represents a comprehensive study reflecting advances in modern laser physics. Considered topics are intended to meet the needs of both specialists in laser system design and those who use laser techniques in fundamental science and applied research. This book is the result of efforts of experts from different countries. I would like to acknowledge the authors for their contribution to the book. I also wish to acknowledge Vedran Kordic for indispensable technical assistance in the book preparation and publishing.

How to reference

In order to correctly reference this scholarly work, feel free to copy and paste the following:

T. Oksenhendler and N. Forget (2010). Pulse-Shaping Techniques Theory and Experimental Implementations for Femtosecond Pulses, Advances in Solid State Lasers Development and Applications, Mikhail Grishin (Ed.), ISBN: 978-953-7619-80-0, InTech, Available from: http://www.intechopen.com/books/advances-in-solid-state-lasers-development-and-applications/pulse-shaping-techniques-theory-and-experimental-implementations-for-femtosecond-pulses

INTECH
open science | open minds

InTech Europe
University Campus STeP Ri
Slavka Krautzeka 83/A
51000 Rijeka, Croatia
Phone: +385 (51) 770 447
Fax: +385 (51) 686 166
www.intechopen.com

InTech China
Unit 405, Office Block, Hotel Equatorial Shanghai
No.65, Yan An Road (West), Shanghai, 200040, China
中国上海市延安西路65号上海国际贵都大饭店办公楼405单元
Phone: +86-21-62489820
Fax: +86-21-62489821

© 2010 The Author(s). Licensee IntechOpen. This chapter is distributed under the terms of the Creative Commons Attribution-NonCommercial-ShareAlike-3.0 License, which permits use, distribution and reproduction for non-commercial purposes, provided the original is properly cited and derivative works building on this content are distributed under the same license.

IntechOpen

IntechOpen